UNIVERSITY OF OKLAHOMA

GRADUATE COLLEGE

A LINDENMAYER SYSTEM-BASED APPROACH FOR THE DESIGN AND

FABRICATION OF NUTRIENT DELIVERY NETWORKS IN TISSUE

CONSTRUCTS

A DISSERTATION

SUBMITTED TO THE GRADUATE FACULTY

in partial fulfillment of the requirements for the

Degree of

DOCTOR OF PHILOSOPHY

By

OZLEM YASAR
Norman, Oklahoma
2011

A LINDENMAYER SYSTEM-BASED APPROACH FOR THE DESIGN AND
FABRICATION OF NUTRIENT DELIVERY NETWORKS IN TISSUE
CONSTRUCTS

A DISSERTATION APPROVED FOR THE
SCHOOL OF INDUSTRIAL ENGINEERING

BY

Dr. Binil Starly- Chair

Dr. Shivakumar Raman

Dr. Randa Shehab

Dr. Chen Ling

Dr. Kuang-Hua Chang

Dr. Zahed Siddique

This thesis has been dedicated to

my wonderful parents,

my mom, Semiha

and

my dad, Habip

with respect and love…

iv

for his patience and support. I could not have completed this dissertation without them.

I love you all and I feel I am lucky to have all of you in my life.

TABLE OF CONTENTS

LIST OF TABLES

LIST OF FIGURES

ABSTRACT

A Lindenmayer System-Based Approach for the Design and Fabrication of Nutrient Delivery Networks in Tissue Constructs for Maskless Photolithography

Ozlem Yasar
Binil Starly, Ph.D

Remarkable advances in the fields of biomedical engineering, material science, molecular biology and biochemistry have made contributions for the cross-disciplinary field of tissue engineering. The field of tissue engineering applies the engineering and the life sciences principles to seek man-made replacements for damaged tissue or whole organs. Porous scaffolds are considered as the key components of tissue engineering because in the regenerative process porous scaffolds guide cells for attachment, proliferation and differentiation in the desired tissue. In today's technology, large thick tissue constructs have reported limited success primarily due to the inability of cells to survive deep within the scaffold. On the other hand, without access to adequate nutrients, cells placed deep within the tissue construct will die out, leading to non-uniform tissue regeneration. Currently, there is a necessity to design nutrient conduit networks within the tissue construct to enable cells to survive in the matrix. However, the design and fabrication of complex networks within a tissue construct is a challenging process.

In this work, we have explored the use of Lindenmayer Systems (L-Systems), a fractal-based language algorithm framework, to generate nutrient conduit networks in two and three-dimensional architecture with several degrees of complexity. The architecture is based on a set of pre-determined axioms and production rules that guide the growth of the conduit networks. The conduit network maintains a parent–child

relationship between each branch of the network. This thesis reports research addressing some of the challenges and proposed solutions in applying the Lindenmayer Systems for the design and freeform fabrication of tissue scaffolds with inbuilt network branches. In addition, we present a maskless photopolymerization based layered manufacturing concept to fabricate the L-System networks in polymeric hydrogels. The major research accomplishments reported in this thesis include:

i.   Development of the Lindenmayer Systems to generate pre-designed nutrient branched networks within the scaffold architecture

ii.   Development of a Digital Light Processing (DLP) setup based on a layered manufacturing photopolymerization system to realize the designed architecture at multiple scales

Lindenmayer Systems enable many novel approaches in modeling and design of complex branching network systems for tissue scaffolds to provide sufficient nutrients distribution for the cells. DLP based layered fabrication also enables researchers to realize precise control of internal architecture design of scaffolds. Since existing design and fabrication techniques lack sufficient nutrient and oxygen delivery deep into the thick scaffolds, we believe that this research will make significance contributions to scaffold based tissue engineering and regenerative medicine. Future research efforts will be undertaken to explore the development of parametric L-System axioms and rules through the use of pre-defined growth functions which allow the branch structure to grow based on the external availability of nutrients and initial input conditions. The goal would be to design scaffold internal architecture designs which take into account manufacturing process constraints while allowing maximal control on the growth of the

branched networks. It is hoped that by providing complex internal patterns that mimic the cellular structure, cells can be guided to form the intended structure. On the manufacturing front, the system will need to be automated to provide a fully integrated SFF system capable of repeatable and stable fabrication process through accurate modeling and control of the various fabrication parameters.

CHAPTER 1 : INTRODUCTION

1.1.   Tissue Engineering

Organ or tissue loss is one of the most common outcomes of disease process, trauma or congenital anomalies. In today's world both shortage of available organ and the number of patients suffering from organ failure has increased day by day. Not only the fact that lack of organ functionality has an important affect on a patients' life quality, but also the high demand for tissue and organ replacement produced a research interest on Tissue Engineering. Basically Tissue Engineering is a promising field which combines engineering principles with biological sciences toward the development of functional substitutes for damaged tissue. Tissue Engineering is strongly linked with application of repair some portion or whole tissues such as bone, cartilage, skin and blood vessels.

As it will be explained in detail in Section 1.3 scaffolds are considered the key parameters of Tissue Engineering. Cells attach to the scaffolds to reorganize themselves to form a tissue. Scaffolds are mostly made of biocompatible polymers and as explained schematically in Figure 1.1 once tissue constructs are implanted to the body, scaffolds degrade away as cells make their own reformations.
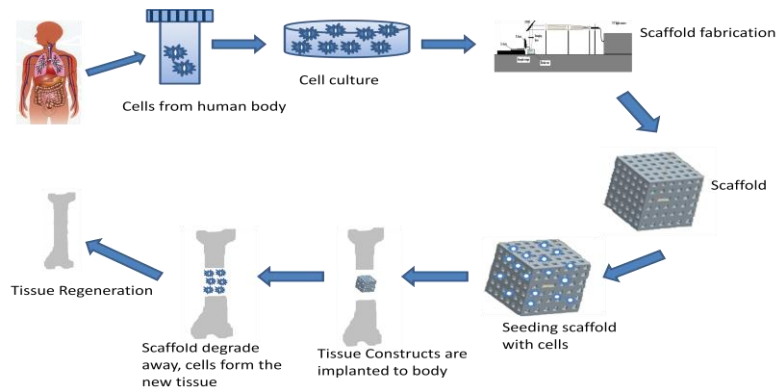
Figure 1.1 Scaffold Based Tissue Engineering.

The use of scaffolds for tissue engineering applications have led to the development of different systems for the deposition of polymers. For instance Khalil et al (2005), Poncelet et al (1999), Calvert et al (1998), Landers et al (2002), Vozzi et al (2002) and Wang et al (2004) did the research on how the deposition of polymers can be controlled through various techniques for the fabrication process.

Langer (2000), Langer et al (1993), Vacanti et al (1999) and Khalil et al (2005) agreed on that tissue engineering is considered to be the most innovative approach for tackling many diseases and body parts that need to replaced. Currently, researchers like Eaglstein et al (1998) have achieved success in growing human skin. Likewise Atala et al (1992) did the study on human urinary bladders and showed promising results. Another significant result was obtained by Sumide et al (2006). Researchers also focused on the regeneration of human internal tissues/organs such as bone, liver and kidney for the clinical applications.

1.2. Tissue Engineering Research Areas

Since the current demands for organ and tissue transplantation is far outpacing, Tissue Engineering is proposed as an alternative way for the treatment of organ transplantation. Tissue Engineering researchers have put the effort in the following areas to meet the current necessities for organ regeneration: Biomaterials, Cells, Engineering design aspects, biomedical design aspects and bio-molecules.

1.3. Significance of Scaffolds for Tissue Engineering Applications

One of the key points behind the tissue engineering involves growing the appropriate cells into the required three-dimensional tissue. Naturally cells lack the ability to grow in three-dimension and they randomly grow and form a two-dimensional shape. However, three-dimensional cell growth is one of the most important requirements for tissue engineering. As suggested by Langer and Vacanti (1993) in order to handle this problem, cells should be seeded into an artificial 3-dimensional porous structure. These structures are called "scaffolds" and they play a vital role in tissue engineering. Scaffolds provide the necessary support for cells to attach, migrate and proliferate into the desired tissue. Ultimately, the scaffolds' external and internal shape also defines the shape of the new organ. There are some important factors has to be taken into account for polymer scaffolds. These basic factors are given by Sachlos et al (2003) and Peter X. Ma (2004)

1. Scaffolds should have interconnected pores and vascularization system to allow cell growth to penetrate into three-dimensional matrices. They also have to be designed at appropriate scales.

2. Materials chosen for scaffolds have to be biodegradable and when they degrade away they should not leave harmful toxic materials behind so that tissue replaces the desired tissue.

3. Scaffolds should have correct surface structure and chemistry for cell attachment, proliferation and differentiation.

4. Scaffolds must have the required mechanical reliability.

5. They must be easily fabricated with variable shapes and sizes.

In tissue engineering the target success can be obtained only cells, engineering and material principles combined together. On the other hand, biological tissues require a network of blood vessels to successfully exchange the nutrients and oxygen with catabolic products. Vozzi et al (2004) suggested that when blood vessels are damaged, the biological tissues can generate new micro vessels. According to Zamir at al (2001) another important role of vasculature system is to reach the certain destinations with the appropriate quantities of blood supplies. However, in today's technology, current fabrication techniques are not capable to create and control the interconnected micro capillary systems inside the scaffolds. Even if well distributed network system is built inside the scaffolds, only simple shapes such as $0\text{-}90^{0}$ structures can be controlled precisely. The limitation of this structure is the pores are filled up with the cells and this prevents the oxygen and nutrients flow deep into the scaffolds. Recently some research groups such as Golden et al (2007), Nelson et al (2006), Chrobak et al (2006), Cabodi et al (2005), Vernon et al (2005), Arcaute et al (2006) and Kaihara et al (2000) have proposed the use of microfluid hydrogels as scaffolds for the transport of materials. However, their method was limited to planar networks.

4

These limitations encouraged researchers to establish a viable technology for built-in oxygen distribution networks for thick scaffolds. According to Folch and Toner (2000), one of the biggest advantages of working with microfluidic systems is to control the cell-cell, cell substrate and cell-medium interactions. According to Rago et al (2009), Hansen et al (1998), Svendsen et al (1998), Akiyama et al (2006) and Korff et al (1998) cell viability and function in 3D can be significantly improved due to the maximization of cell to cell contacts. There have been different experiments done where microchannels used as flow microenvironments to test the cell growth for tissue engineering. For instance, flow and oxygenation on hepatocytes was studied by Tilles et al (2001) and Roy et al (2001). Similar experiment was done by Gemmiti and Guldberg (2006) to investigate the oxygen transport by flow and to test the mechanical properties of scaffolds for cartilage regeneration. In our research we designed a scaffold with inbuilt network system as shown in Figure 1.2.
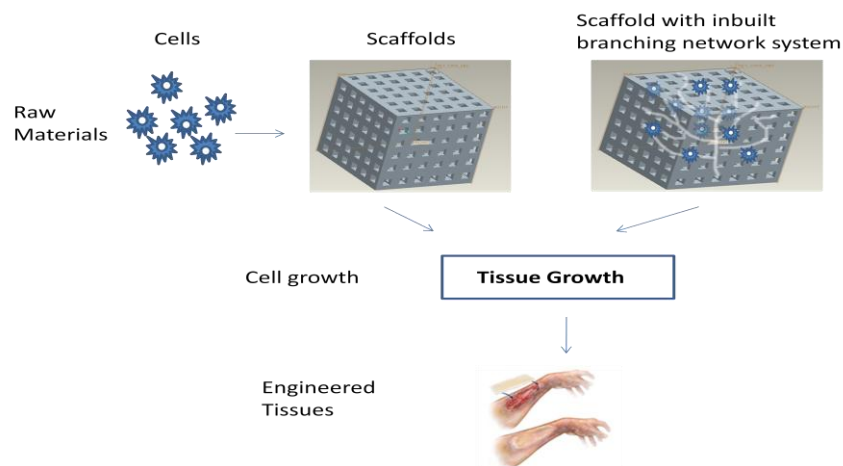
Figure 1.2 Overview of Engineered Tissue. Cells attach and migrate on the 3-D scaffold to form a desired engineered tissue.

5

1.4. Scaffold Fabrication Techniques

1.4.1. Traditional Scaffold Fabrication Techniques

Porous scaffolds can be fabricated using variety of fabrication techniques. Solvent casting and particulate leaching, gas foaming, melt molding and solution casting can be given as an example of some of these fabrication techniques. The biggest limitations of these traditional fabrication techniques are uncontrollable internal architecture design and uncontrollable homogeneity and accuracy. Since the fabrication method significantly affects the properties of the implant and the degradation characteristics correct fabrication technique should be chosen. Some of the advantages and the disadvantages of these fabrication techniques were summarized by Yang et al (2001) and Buckley et al (2004) and were shown in Table1.1. In general success for these fabrication techniques depends on the material used to fabricate the scaffold and its intended application Karina et al (2006), Lu et al (1996) and Ma (2004). These traditional fabrication techniques are defined in this chapter.

1.4.1.1. Solvent Casting and Particulate Leaching

Mikos at al (1994) explained that solvent Casting and Particulate Leaching method consists of dispersing calibrated minerals such as sodium chloride, tartrate and citrate or saccharose like organic particles in a polymer solution. After the solvent is allowed to evaporate to leave the polymer matrix with salt particles behind the composite is immersed in water to allow salt leaches out to produce a porous structure.

6

1.4.1.2. Gas Foaming

Mooney et al (1996) worked on gas foaming technique and in this fabrication method they used a biodegradable polymer such as PLGA and under the high pressure they saturated it with carbon dioxide. After that CO_2 pressure is brought to the atmospheric level and this step decreases the solubility of the gas inside the polymer which produces the different size gas bubbles.

1.4.1.3. Melt Molding

In the melt molding process fine PLGA powder is mixed with the gelatin microspheres and it is loaded in a teflon mold. It is then heated to the above the glass-transition temperature of the polymer. At the same time high pressure is applied to the mixture to bond the PLGA particles. As a last step mold is removed and gelatin is leached out in the water. Since the polymer scaffold shape depends on the geometry, by changing the mold different shape of scaffolds can be fabricated. L-PLA and PGA can also be used instead of PLGA. In case of using L-PLA or PGA higher temperature is needed to melt the semicrystalline polymers.

1.4.1.4. Solution Casting

This method was used by Sachlos et al (2003), Reuber et al (1987) and Schmitz and Hollinger (1988). In order to create the scaffolds with solution casting PLGA is dissolved in chloroform and precipitated by methanol. After that demineralised freeze-dried bone is combined with the PLGA and high pressure is applied into a mold and it is heated to 45 to 48^0C for 24 hours.

7

Table 1.1 Advantages and disadvantages of traditional fabrication techniques were summarized by Yang et al (2001) and Buckley et al (2004).

Process	Advantages	Disadvantages
Solvent casting and particulate leaching	• Large pore sizes • Controlled porosity up to 93% • Independent control of porosity and pore sizes • Highly porous structures	• Limited membrane thickness (3mm) • Lack required mechanical strength • Harmful solvent residue • Poor control of internal structure
Melt Molding	• Independent control of porosity and pore size • Macro shape control	• High temperature for nonamorphous polymer
Fiber Felts	• Easy process • High porosity	• Poor structural stability
Phase Separation	• Highly porous structures • Incorporation of bioactive agents	• Poor control of internal architecture • Limited range of pore sizes

Scaffolds with the foam structures can be produced by the traditional fabrication techniques. Seeded cells onto these scaffolds are expected to grow. However, Ishaug-Riley et al (1997) and Freed et al (1998) showed that due to the diffusion constrains of the foam only the tissues with the cross-sections less than 500µm can show a success for tissue growth. Figure 1.3 represents the diffusion constrains inside the foam like

8

scaffold structures. As shown in Figure 1.3 oxygen and nutrients flow in the arrow direction to help cells to grow, proliferate and migrate. However, only the cells on the surface of the scaffolds consume oxygen and grow. Once the cells at the exterior of the scaffold start growing, they block the porous and this prevents the oxygen and nutrient flow to the interior of the scaffold. Due to the lack of oxygen and nutrients cells die out at the interior part of the scaffold. Cells only survive in the penetration depth D_p area. In order to provide oxygen and nutrients to the cells inside the scaffolds inbuilt vascularization system is needed.

Cell culture medium

D_p

| (a) | (b) | (c) | (d) | (e) |
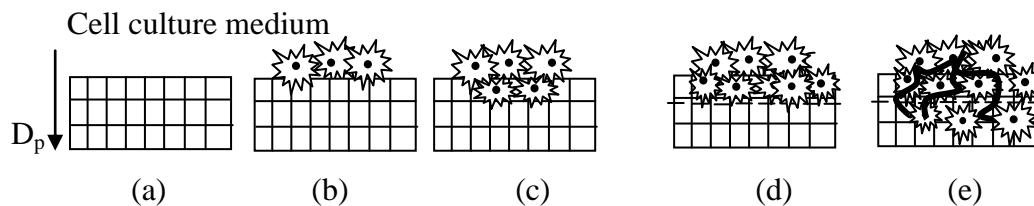
Figure 1.3 (a) Foam like scaffold, O_2 and nutrients flow is in the arrow direction (b) Cell seeding on the scaffold (c) proliferation and migration of the cells (d) Cells on the top of the scaffold consumes more oxygen and the nutrients than the cells in the middle. (e) Artificial vascularization system is needed to provide the sufficient oxygen and nutrients to the cells inside the scaffolds.

1.4.2. Solid Freeform Fabrication (SFF) Techniques

Current research encouraged investigators to work on the rapid prototyping (RP) or solid freeform fabrication (SFF) technologies. According to Vozzi and Chione et al (2004), Zein et al (2002) and Lam et al (2002) RP are developing to fabricate scaffolds with controlled architectures. Also SFF is the key to produce scaffolds with controllable

external and also the internal shape. SFF let researchers to control internal morphology such as pore size, pore distribution and porosity.

The basic principle of SFF methods is to solidify either powder or liquid material as a single layer and this process is repated for multiple layers to obtain the 3D shape. Thus SFF technologies are an additive manufacturing process unlike traditional methods which are subtractive based. The principle of SFF based technologies work by firstly obtaining a computer based 3D model designed with computer aided design (CAD) software and then the 3D model is divided into thin cross-sectional slice layers. After that, the data is sent to the SFF machine and each layer is created from bottom to top. After the completion of the first layer, SFF platform is moved to down with a step of one layer and second layer is created. Each layer is adhered to the previous one till the whole shape is completed. The most common SFF technologies are stereolithography (SLA), selective laser sintering (SLS), fused deposition modeling (FDM) and three dimensional printing (3DP).

1.4.2.1. Stereolithograph (SLA)

The main components of SLA are x-y axis control UV beam, photo-curable monomer solution, CAD data and z-axes controllable elevator. As shown in Sachlos' paper et al (2003), according to CAD data, the UV beam is guided onto the monomer solution and as an interaction between the UV light and the monomer solution, photopolymerization occurs and the first layer is built. After that z-elevator which holds the first layer is lowered into the monomer solution in the z direction and the procedure

is repeated until the whole model is completed. Figure 1.4 represents the schematic of streolithography process.
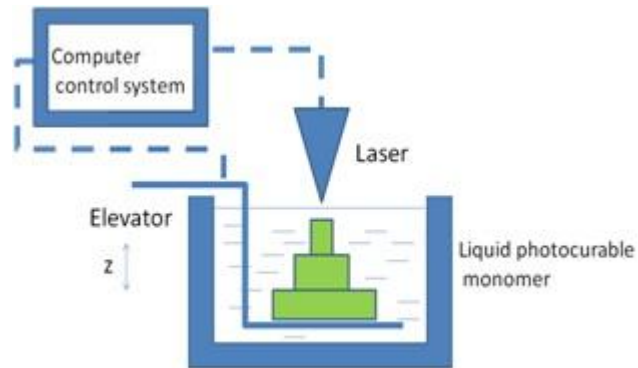
Figure 1.4 Streolithography Schematic Diagram

1.4.2.2. Fused Deposition Modeling (FDM)

As shown in Figure 1.5. Sachlos et al's paper (2003) described the FDM process as an x-y axis controllable moving nozzle system which extrudes polymeric material in the desired layer thickness. Produced layers are lowered in the z-direction and all the steps are repeated until the last layer.
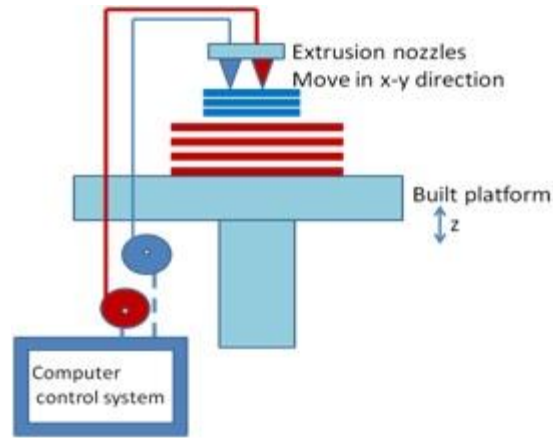
Figure 1.5 Representation of FDM schematic diagram

1.4.2.3. Three-Dimensional Printing (3DP)

3DP has a removable jet had which eject the binder on the polymer powder surface according to CAD data. This jet head can be removed both in the x and y directions. Polymer powders are dissolved and stick to each other to produce the first layer. The piston is lowered in the z-direction and fresh powder particles refill the printer's surface. The same procedure is repeated to make the other layers on the top of the previous one. 3DP diagram is represented both in Figure 1.6 and also Sachlos et al's work (2003).
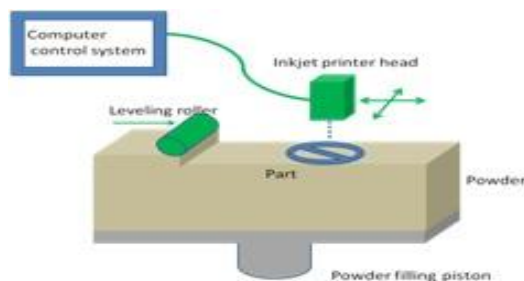
Figure 1.6 Schematic diagram of 3DP

1.4.2.4. Mask Based Photolithography

Photolithography is one of the fabrication techniques that use the light to create a pattern. With UV light (370nm) pass through a photo mask and creates a geometric pattern on the substrate. In this system according to mask design only selective parts are removed from a bulk of substrate and desired patterns are produced. Figure 1.7 summarizes the photolithography steps to create the micro-patterns.
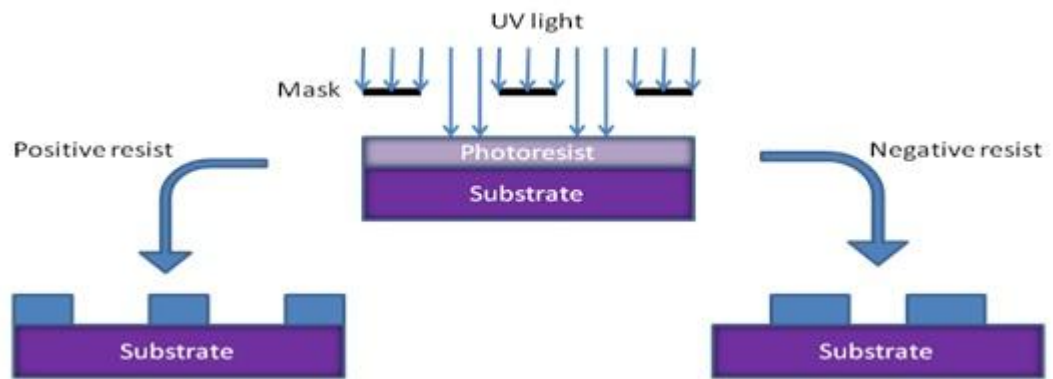
Figure 1.7 Schematic diagram of photolithography process.

Currently these SFF techniques have been used by different research institutes and laboratories. In the following table the flexibility, advantages and limitations of SFF techniques are compared, reviewed and summarized.

Table 1.2 Advantages and limitations of SFF fabrication techniques were summarized

in Buckley et al's work (2004).

Process	Advantages	Limitations
SLA	• Easy to remove support materials • Easy to produce small features	• Only photopolymerizable, biocompatible and biodegradable polymers can be used
FDM	• Materials are not trapped within the small features	• Requires support for irregular structures
3DP	• Different kind of materials can be used	• Powder particles block the small internal features • Toxic organic solvents are used • Lack of mechanical strength

1.5. Research Motivation

One of the biggest challenges that medical doctors and researches face in today's technology is organ transplantation. This is due to the fact that finding a right donor organ is very exigent, time consuming and costly. Organ transplant statistics show that each day, in the US, average 18 people are dying because of the shortage of

donor organs and in every eleven minutes a new person is added to the waiting list to find a donor organ (http://www.donatelifeny.org/about-donation/data/). Tissue Engineering plays critical role in this point because tissue engineering researchers apply the principles of engineering and life sciences to develop biological substitutes to restore, maintain or improve tissue function or whole organ. In order to be successful to do the tissue regeneration 3-D microenvironments called scaffolds are needed to provide the cell attachment and cell proliferation. Scaffolds are key parameters for tissue engineering researches as they are the skeletons for cells to grow and treat the critical size defects. Currently, to design and fabricate the scaffolds thicker than 5mm is tricky as the chance of accessibility of nutrients deep into the scaffold is not sufficient for cells to survive. In order to handle these problem thick scaffolds must have an inbuilt 3-D nutrient distribution network to facilitate the delivery of nutrients for the uniform cell growth within the scaffolds until the cells themselves are capable of creating their own vasculature network.

1.6. Research Objective

As explained earlier, thicker scaffolds must have an inbuilt 3D nutrient distribution network to facilitate the delivery of nutrients for the uniform growth of cells within these man-made matrices until the cells themselves are capable of creating their own vasculature network. The specific research objectives of this research are:

i. To develop Lindenmayer Systems methodology to generate pre-designed nutrient branched networks within the interior architecture of scaffold geometry. In this research we have attempted to define the necessary L-Systems

axioms and rules to generate the nutrient conduit architecture. We have studied the effect of several L-Systems parameters on the geometrical definition of the L-Systems framework.

ii. To develop an appropriate layered manufacturing system to fabricate the designed L-Systems nutrient conduit architecture. We used a maskless photolithography setup to fabricate multi-layered hydrogel scaffolds based on poly-ethylene glycol diacrylate (PEGDA) with spatially distributed branching networks. This system enables the fabrication of fine features at micron scales. Experimental studies were conducted to investigate the effect of process parameters on hydrogel fabrication.

1.7. Thesis Outline

This thesis is outline as explained in the following:

Chapter 2 gives the whole detailed information about the use of L-Systems, which represents a structure as a string of axiom and rules, for the design of nutrient delivery networks. In this chapter, how L-Systems are used to generate and control the branching network systems is also explained in detail. Influence of L-System parameters on branching properties such as orientation, thickness and length is also investigated. Comparison of Murray's law with L-Systems is also explained to show the superiority of L-Systems over Murray's law.

Chapter 3 describes the DLP based fabrication of hydrogel scaffolds. In this chapter first of all maskless photolithography setup was clarified. Manufacturability of the unfilled nutrient delivery networks and layered maskless photolithography process

is explained. Effect of maskless photolithography parameters on hydrogel accuracy is also studied with different examples in Chapter 3.

Chapter 4 contains the information about cellular encapsulation using DLP based maskless photolithography. How HepG2 cells were used to do the cell encapsulation is investigated. Fabrication of hydrogel structures containing HepG2 cells is clarified.

At the end of this thesis, conclusions, recommendations and what can be done in the future as an extension of this research is represented in Chapter 5.

CHAPTER 2: LINDENMAYER SYSTEM ARCHITECTURE

2.1. Lindenmayer Systems

Lindenmayer Systems were developed by theoretical botanist Aristid Lindenmayer in 1968 and are most commonly used in the graphical modeling of the growth and development of plants, bacteria and algae. An L-system framework represents a structure as a string of symbols, termed the axiom, which at every successive rewriting step can be transformed using a matching production rule. This process is used to expand the string of symbols and can be interpreted visually. For example, an axiom is defined as 'B' and the production rules are set to be such that in successive rewriting steps, all Bs are replaced by 'A' and all As are replaced by 'AB'. Repeating the rewriting process iteratively for a finite number of steps, a sequence of strings is generated that are replaced simultaneously at each step of the process As shown in Figure 2.1 due to this parallel rewriting mechanism, L-systems have the capability to model biological phenomena such as branching network systems and cell growth. It will be also explained in detail how one can control the orientation, thickness, length and the number of branches with Lindenmayer Systems.
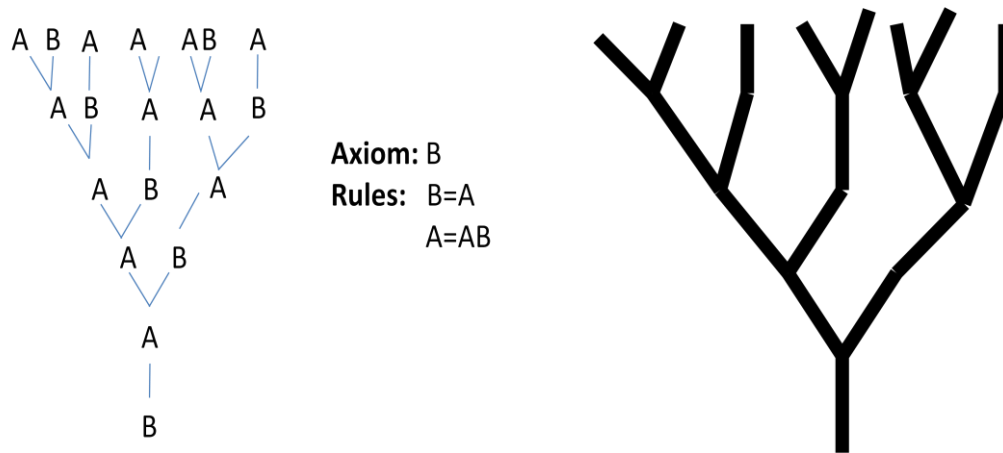
Figure 2.1 Lindenmayer systems to produce branching network systems.

If axiom is defined by F, turning angle θ is given 60^0 and if the rule is stated F will be replaced by F+F- -F+F; first 2 iterations are represented as shown in Figure 2.2

Axiom: F	——————	**Iteration 0**
Production Rule: F→ F+F- -		Iteration 1
F+F		
θ Turning angle = 60⁰		
		Iteration 2
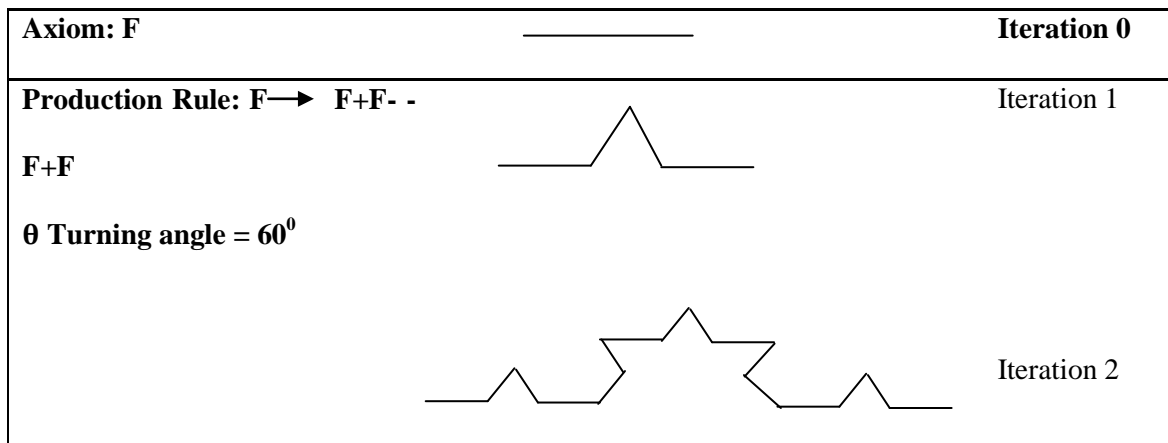
Figure 2.2 Koch Curve L-System. In each iteration all the Fs are replaced by reduced copy of the previous one.

Starly et al (2007), Karch et al (2003), Beard et al (2000) and Buijs et al (2006) emphasized that a number of techniques are currently available to model the vasculature system which are fractal based techniques and they are most commonly used to address

19

the circulatory diseases. According to Freed et al (2006) L-systems can be extended to geometric interpretation using Turtle graphics, to generate fractal curves, space filling curves and plant like structures. The position of turtle is given in Cartesian Coordinates and the orientation of turtle is given by angle of θ. The symbols which cause to move and draw a line with step of length s are F(s) and f(s). The difference between F(s) and f(s) is, specified step distance s is drawn with the notation of F(s) whereas turtle only move forward without drawing a line with the notation of f(s). Similar symbols are available for a full 3D orientation of the axiom production. A description of all turtle symbols are provided in articles published by Prusinkiewicz et al (1990).

Table 2.1 illustrates some of the meanings of symbols used in L-systems by Prusinkiewicz et al (1990) (1996).

Table 2.1 Meaning of L-System symbols

L-System Symbols	Meaning
F(s)	Move forward and draw a line with step length s
F(s)	Move forward with step length s, do not draw a line
+(θ)	Turn left by angle θ
-(θ)	Turn right by angle θ
\(θ)	Roll left by angle **θ**
/(θ)	Roll right by angle **θ**
^(θ)	Pitch down by angle **θ**
&(θ)	Pitch up by angle θ
|	Turn around with 1800
[	Push current drawing state onto stack
]	Pop current drawing state from the stack

With these rules the string which causes the turtle movement and controlling the branch orientation can be obtained. For instance if it is assumed that the turtle is initially facing upwards, the axiom of FFF+F+FF-FF+F-FFF causes the following outline

Axiom: FFF+F+FF-FF+F-FFF

Figure 2.3 "L" shape turtle configuration with assuming the turtle is initially facing up.

2.2. Use of Lindenmayer Systems for the Design of Nutrient Delivery Networks

Advantages in L-systems make it possible to visualize realistic tree models starting from trunk to branching structures. Linsen et al (2005) and Honda (1971) has explained that this application permits the description of the geometrical properties of branching systems such as number of the branches, length of the branches, their radius and branching angles. The fundamental nature of model development with L-system is rewriting organization which repetitively replaces the main part by configuration of daughter branches.

Consider that we are required to model a simple Y-shape branch structure through an appropriate L-system notation (axiom and production rule). To satisfy physiological necessities such as nutrient distribution of the surrounding matrix, let us assume a dichotomously branching structure with a total of 'T' segments. The geometrical parameters of the branch networks are given as follows: each bifurcation is associated with a cylinder (with constant radii, r, against an input inlet nutrient species concentration, C_{in}). The distal end (downstream point) of each segment is given by the coordinates $P(x_i , y_i , z_i))$ where $1 < i < T$. The ratio, R_{length}, is defined as the ratio of the

length of the bifurcating child segment to the length of the parent segment (L_2/L_1). θ_1 and θ_2 are angles which the child branch segments make with the central axis of the parent segment. The sweep angle (top view) of the bifurcating branches is given by α_1 and α_2 as shown in Figure 2.4(b).
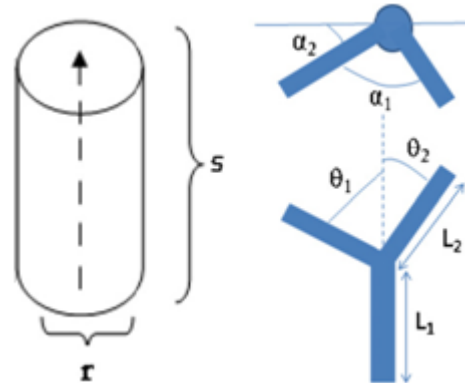
Figure 2.4 (a) Simple unit branch; (b) network bifurcation parameters (θ_1, θ_2, L_1, L_2, α_1, α_2).

Each segment of the network will have associated topological features such as index information of the parent segment and a link to its own children and sibling segments. These parameters can be used to define a basic branch within an L-system framework, through which more complex branches are created. This basic branch is termed the representative branching element (RBE). RBEs are iteratively expanded to form the entire conduit structure.

A parametric branching network L-system, $G(\omega, \Sigma, P, V)$, is specified by four components: (a) an initial axiom, ω, which represents the nutrient conduits during the first execution of the L-system to form the RBE structure; (b) a formal user defined set of parameters given by 'Σ', which is passed onto the axiom; (c) a set of branch

production rules, P, which repeats the structured growth of the RBE based on a set of conditional constraints and (d) the alphabet, V, of the system which defines the geometric and topological arrangement of the branches. Each parameter in the axiom, ω, can store information about the growth of the structure. For example, an axiom ω =A(v_1, v_2, v_3) can accept three parameters during the rewriting procedure, which at every stage can carry over information from one step to the successive iterative step. Each user-defined parameter can store a list of the segment properties. This can then enable attributes from the parent to be transferred to the child while ensuring conformity with the external physical environment. For example, a simplistic parametric L-system, G, shown in Figures 2.5(a)–(b) defines a 2D growth of nutrient conduits. As Starly et al (2007) explained in detail, a similar notation can be written for the growth of the branches in 3D within an enclosed volume.

```
#define R=0.8
#define N=10
#define L1=1000

W: A(L1)
Begin Loop
P₁: A(s): s>600     F(s)[+A(s*R)][-A(s*R)]
End loop
```

(a)   (b)   (c)
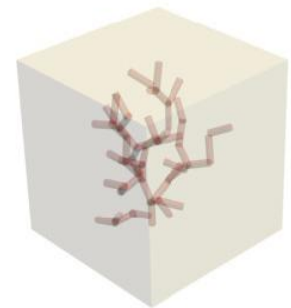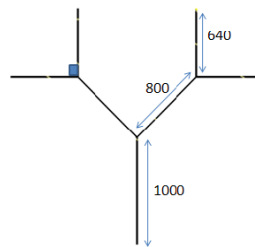
Figure 2.5 (a) Sample parametric L-system; (b) Geometric 2D representation of the L-system in (a); (c) rendering of the 3D branched networks.

In this example, the axiom accepts the input parameter L_1 =1000μm, as the length of the first segment. L1 is assigned to the variable 's'. The conditional statement

24

(s > 200) checks to see if the length of the segment satisfies the condition. If it does, the production rule, P1, is applied as shown by the characters to the right of the arrow. Each successive segment length is reduced by a factor 's*R'. The process continues until either N = 10 is reached or the condition turns out to be false. In the example shown, the process stops at step N = 3 due to the conditional statement being false. It would also be possible to include multiple production rules which are applied based on the value of the parameters. A similar L-system notation can be derived to generate branched networks in the third dimension.

2.2.1. Computer Environment for L-System Definitions

Similar to Karwowski and Merch's work (1996), in this research L-Studio which is simulation software for modeling the virtual experiments using L-Systems to provide the mathematical framework to create branching structures with varying constants in each production steps was chosen. Simulations were executed using lpfg, which is a built-in program for simulation software L-studio. The model was written with L+C language. It is also possible to visualize the simulation results from different angles in 3-D with the help of L-studio by Mundermann et al (2005)

2.2.1.1. Influence of L-System Parameters

As explained earlier using the L-system notation, we have defined our own axiom to reflect the applicability of the process to mimic a vasculature network reconstructed from MRI images. Figures 2.6(a)–(b) show an MRI image of a vasculature network within a rat portal kidney and portal vein, respectively. Data from

the reconstructed model are retrieved to enable the input of the several L-system parameters. For example, data such as the diameter of the root, number of offshoots from main branch, angle of offshoot with the main branch axis, length of the offshoots, levels of branches, ratio of child branch to parent branch diameter were collected. These data were then translated into L-system parameters which drive the notation scheme. To illustrate the usefulness of the L-system framework, we have come up with the appropriate L-system notation to biomimic the structure shown in Figure 2.6 (b). The L-system notation is as shown below. The final L-system reconstructed model is shown in Figure 2.6.(c).

(a)   (b)   (c)
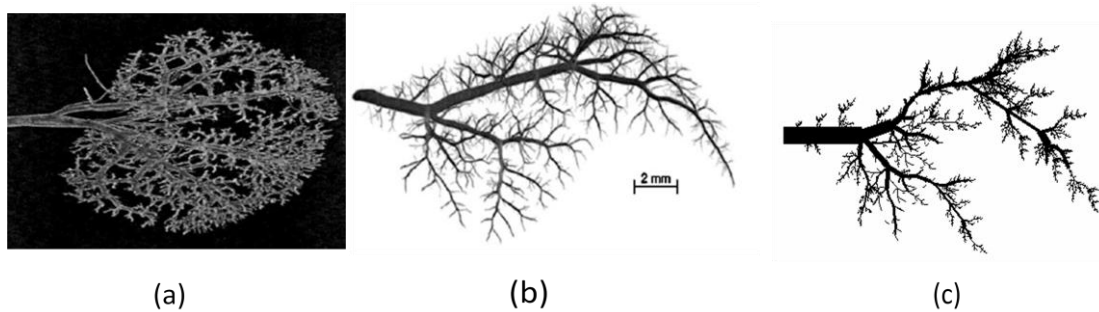
Figure 2.6 (a) Vasculature network of rat kidney; (b) vasculature network of a rat portal vein; (c) L-system design of the vasculature network of a rat portal vein shown in (b)

Although verbose in the definition of the axiom, the notation becomes very powerful when defining complex branch structures. In this notation, the diameter of the branch diameter can be varied through each production step. This is defined by a constant ratio of the child branch to the parent branch. The use of stack operators '[' and ']' allows branches to originate from previously stored locations. This enables branching of a parent branch into offshoot structures.

26

```
#define STEPS 4    #define a_1 50    #define a_2 35    #define r1 0.1    #define r2 0.15
#define r3 0.3      #define r4 0.5    #define q 0.1        #define e 0.5      #define k 0.3
#define l 0.2      #define m 0.01    #define omega_0 18  #define min 0.0

Lsystem: 1

Axiom: A(100,omega_0)

A(s, w): s --> !(w)[f(s)+(a_1)A(s*r1,w*q)] [f(s*3)+(a_1)A(s*r2,w*q)]
[f(s*5)+(a_1)A(s*0.25,w*q)] [f(s*2)-(a_1)A(s*r2,w*q)] F(s)[f(s)+(a_1)A(s*0.2,w*q)]-(27)[-
(20)[A(s,w*e)][f(s)+(a_1)A(s*0.7,w*q)] [-(a_1)A(s*r4,w*k)]]  +28A(s*0.8,w*0.7)[55A(s*0.4,w*0.25)]
[[+75A(s*0.4,w*k)][+95A(s*r4,w*k)] [+120A(s*0.6,w*k)]] F(s*0.6)[+25A(s*r3,w*l)][-
a_2A(s*r3,w*l)]   F(s*0.5)[+35A(s*r3,w*l)][-a_2A(s*r3,w*m)] -(25)A(s*r3,w*0.55)[+5A(s*r3,w*m)]

F(s) --> F(s)F(s)

endlsystem
```

Figure 2.7 L-system notation for the branched structure in Figure 2.6 (c).

The length and the width of the branches are determined with 's' and 'w',
respectively. In Figure 2.6 (c), it is noted that through the L-system notation, a 3D
model of the branch networks can be generated without excessive use of graphical
resources and computational power. However, the usefulness of a branched network is
limited since it would be practically impossible to fabricate a branched network with the
level of complexity shown in Figure 2.6 (c). Therefore, our next step was to limit the
growth of the branches based on certain manufacturing constraints set within the
system. An iterative branched network design is postulated with the angle of branches
set to be at 90◦ and shown in Figure 2.8. It is seen that the iterative steps were carried
out until the minimum diameter of any branch was limited to a minimum of 100 μm.
Several variations with different angle and branch diameters can be formulated. To an
extent, the width between the branching elements can be controlled by careful selection
of the L-system parameters.
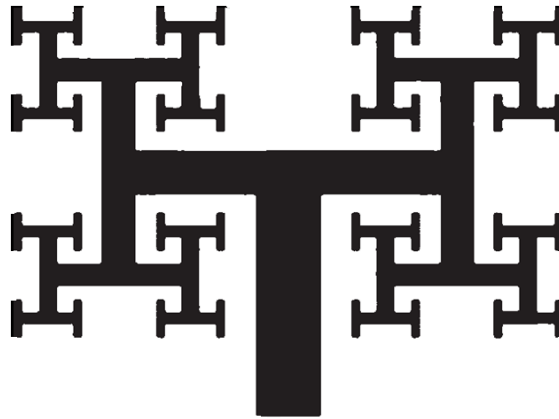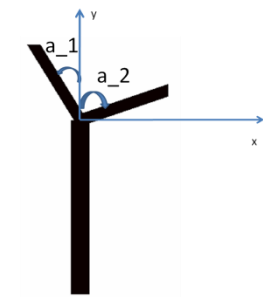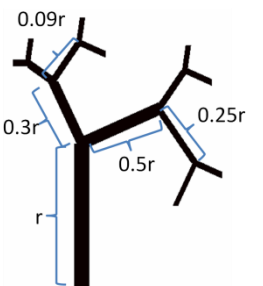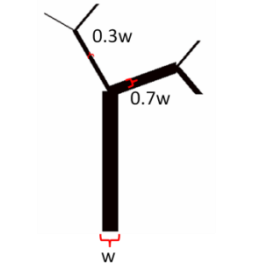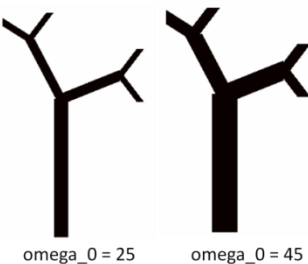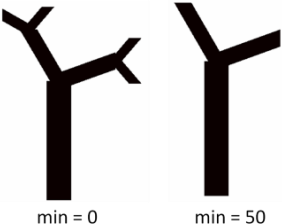
Figure 2.8 Branched pattern with L-system

System design begins with an initial string called axiom A(s, w) which specifies the initial structure as a trunk and two branches. The defined constants help to determine the branch node position, branch orientation, branch width and length. In each rewriting step, the production rules add new branches to the previous ones. The constants a_1 and a_2 represent the orientations of new branches and 'w' sets the initial branch width to 75. The parameters 's' and 'w'determine the internode length and width. The constants 'r_1' and 'r_2' specify the gradual decrease in internode length that occurs while traversing the tree from its base toward the apices. The constant value 'min' prevents formation of new branches with length less than the threshold value min. Here, the constants omega_0 and minimum do not specify actual dimensions but rather dimensionless parameters which relate to the actual obtained dimension during fabrication. Table 2.2 summarizes the influence of L-studio constants on branching network systems.

28

Table 2.2 Influence of L-system notations on branching network system

L-System Symbols	Meaning	Orientation
a_1, a_2	Angle between the branches and y-axis	
r1, r2	Gradual decrease in internode length	
q, e	Control the width of the branches	
omega_0	Initial steam width	
Min	Threshold value to create the branches	

```
#define a_1 90        #define a_2 -90       #define phi_1 0       #define phi_2 0
#define r1 0.65       #define r2 0.65       #define q 0.5         #define e 0.5
#define omega_0 75    #define min 1.7       #define n 1
```

Lsystem: 1
derivation length: STEPS
Axiom: A(100, omega_0)

A(s, w): s >= min --> !(w)F(s) [+(a_1)/(phi_1)A(s*r1,w*q^e)] [+(a_2)/(phi_2)A(s*r2,w*(1-q)^e)]

End lsystem

Figure 2.9 L-system notation with in-built constraints to produce Figure 2.8 design.

Keeping the axiom and the production rule the same, changes in the parameters for the branch network can result in varying network branch orientations. Table 2.3 shows the different variables for the parameters to obtain different branch orientation. In the three different branch structures, it is pointed out that the main RBE structure as defined by the axiom has not changed. Yasar et al (2009) also note that there should exist a clear correlation between the parameters in Table 2.3 and the nutrient diffusion capability of the branched networks. However, this will be studied as a future extension of the current work.

Table 2. 3 Constants for the branching patterns generated by L-systems

	a_1	a_2	phi_1	phi_2	r1	r2	Q	E	N
Figure 2.10 (a)	30	-70	0	0	0.65	0.71	0.5	0.5	8
Figure 2.10 (b)	85	-85	180	0	0.6	0.6	0.5	0.5	7
Figure 2.10 (c)	75	-75	0	0	0.7	0.7	0.5	0.5	7

(a)   (b)   (c)
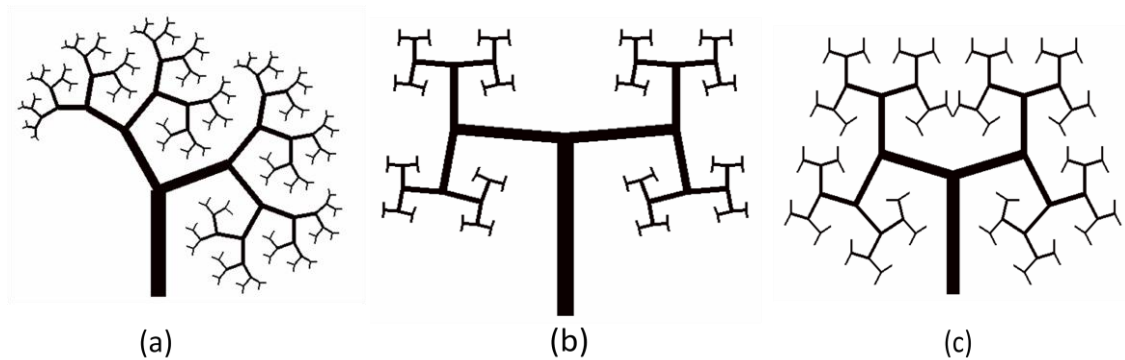
Figure 2.10**.** Branching patterns generated by the L-system specified with the constants

shown in Table 2.3

In order to provide the sufficient oxygen and nutrients for the cells deep into the

scaffolds we have defined a branching network system and we have designed these

network systems with L-Systems. We came up with the axiom and rule definitions to

control the length, width, number, position and orientation of the branches. As shown in

Figure 2.11 we have started our design with a simple "y-shape" structure and then we

took one step further to increase the level of branches.

#define a_1 45 #define r1 0.5 #define q 0.5 #define a_2 -45 #define r2 0.5 #define e 0.5 #define omega_0 30 #define min 10.0 #define STEPS 3 Lsystem: 1 derivation length: STEPS Axiom: A(100,omega_0) A(s,w): s >= min --> !(w)F(s) [+(a_1)/(phi_1)A(s*r1,w*q)] [+(a_2)/(phi_2)A(s*r2,w*e)] endlsystem (a)	(b)	(c)

Figure 2.11   (a) Parametric L-system notations   (b) representation of 2D branching

network system growth for STEP Number 2   (c) representation of 2D branching

network system growth for STEP Number 3

2.3. Comparison of Murray's Law with Lindenmayer Systems

In order to design the branching network system, Murray's law was used by different research groups such as University of Pisa and California Environmental Protection Agency. According to Painter et al (2006) Murray's law states that when a parent branch divided into two different branches, the cube of the radius of the parent branch is equal to the sum of the cubes if the radii of daughter branches.
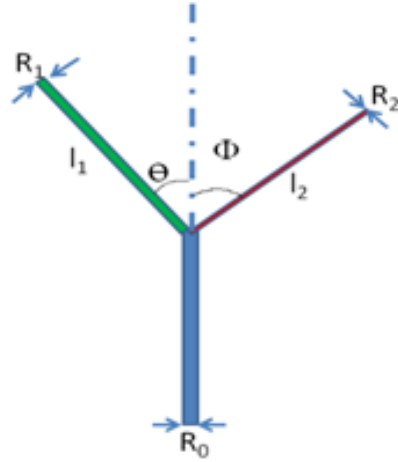
$$\cos \varphi = \frac{R_0^4 + R_2^4 - R_1^4}{2R_0^2 R_2^2}$$

$$\cos \theta = \frac{R_0^4 + R_1^4 - R_2^4}{2R_0^2 R_1^2}$$

$$R_0^3 = R_1^3 + R_2^3$$

Figure 2.12. Schematic of parent and its daughter branches

Vozzi et al (2004) suggested that as shown in Figure 2.12, for a given parent radius R_0 and left hand daughter branch with a radius R_1 and branching angle Θ and right hand daughter branch with a radius R_2 and branching angle Φ, according to Murray, those branches must obey the following formulations

$$\cos\theta = \frac{R_0^4 + R_1^4 - R_2^4}{2R_2^2 R_2^2} \qquad [1]$$

$$\cos\varphi = \frac{R_0^4 + R_2^4 - R_2^4}{2R_2^2 R_2^2} \qquad [2]$$

$$R_0^3 = R_1^3 + R_2^3 \qquad [3]$$

One of the biggest limitations to generate the branching networks with the Murray's law is one branch can only produce two daughter branches whereas with L-systems one parent branch can generate as many branch as necessary. In Vozzi et al's research it is also assumed that the ratio of the radius of the kth level to the (k+1)th level is constant :

$$\frac{R_{k+1}}{R_k} = \beta \qquad [4]$$

Same approximation was also applied to the ratio of the length of the kth level to the (k+1)th level is constant :

$$\frac{l_{k+1}}{l_k} = \gamma \qquad\qquad [5]$$

Table 2.4 shows the basic advantages why of the L-System approach when compared to Murray's law.

Table 2.4 Murray's law vs. Lindenmayer Systems

	Murray's law	Lindenmayer Systems
Number of branches generated by a parent branch	2	As many as we want
Formulations branches must obey	$cos\theta = \dfrac{R_0^4 + R_1^4 - R_2^4}{2R_2^2R_2^2}$ $cos\varphi = \dfrac{R_0^4 + R_2^4 - R_2^4}{2R_2^2R_2^2}$ $R_0^3 = R_1^3 + R_2^3$	No formulation- branch orientation is controlled with axiom
Ratio of the radius of the (k+1)th branch to the kth branch	Constant $=\dfrac{R_{k+1}}{R_k} = \beta$	Not necessarily to be constant it can vary through the branching steps
Ratio of the length of the (k+1)th branch to the kth branch	Constant $=\dfrac{l_{k+1}}{l_k} = \gamma$	Not necessarily to be constant it can vary through the branching steps

2.4. Conclusion

As described by Prusinkiewicz and Lindenmayer (1990) and Prusinkiewicz (1993) Lindenmayer Systems were first developed by botanist Artist Lindenmayer in 1968 and mostly used in the graphical modeling of the plants. The main concept of Lindenmayer Systems is the rewriting process. Due to this parallel rewriting mechanism, L-Systems have the capability to model biological phenomena such as cellular growth by simulating cell division and death. In our research we took advantage of using L-Systems to design and control the branching network systems. The importance of existence of these network systems within the scaffold is to provide the sufficient oxygen and nutrient flow for cells which are located at the interior of the scaffolds. In our research these branching network systems were not produced randomly they were generated according to the L-Systems axioms, rules and parameters.

Branching network design begins with an initial string which is also known as axiom. Axiom determines the initial structure as a trunk and branches. The constants used in the Lindenmayer Systems determine the branch position, branch orientation, branch width and length. In each rewriting step, the production rules add the new branches to the previous ones.

Keeping the axiom and the production rules constant, only by changing the L-System parameters varying network branch orientations can easily be obtained. Table 2.3 summarizes how changing these different variables effect the branch orientation.

Murray's laws are the other way to design the vascularization systems that was used by other research institutes. In our research we preferred to design these network systems with L-Systems as the Murray's law has limitations on designing the branches.

The main advantages of L-Systems compared to Murray's law were summarized in Table 2.4.

As explained by Yasar et al (2009) earlier there is a clear correlation between the L-System parameters and nutrient diffusion capability of the vascularization systems. However, this will be studied at the future extension of this current work.

Chapter 3: DLP BASED FABRICATION OF HYDROGEL SCAFFOLDS

3.1. Maskless Photolithography Setup

Recent advancement in manufacturing methods such as patterning and deposition technologies has enabled researchers to spatially control hydrogel architectural features through the use of soft lithography, photolithography and solid freeform fabrication. These techniques have produced patterned hydrogels with desired chemical and mechanical properties capable of designing biomimetic microenvironments. Soft lithographic techniques have produced feature sizes in ranges of 20 μm and above but have limited 3D capability. Solid freeform fabrication technologies enable the production of complex 3D hydrogels due to their CAD integration but are generally limited to a minimum of 100 μm feature resolutions. Photolithographic methods have produced hydrogels by the direct exposure of the polymer solution to UV radiation to produce micro-patterned scaffolds with feature sizes in the range of 50 μm or more. Until recently, the photolithographic technique had limited capability in producing three-dimensional scaffolds due to the lack of true three-dimensional formation capabilities. Itago et al. (2006) and Sun et al. (2005) proved that, with the development of the maskless projection photolithographic and micro-stereolithography, it is now possible to create complex three-dimensional scaffolds with defined architecture and minimum feature sizes of the order of 50 μm. Maskless projection photolithography has the capability of producing hydrogels with well-defined, repeatable and complex 3D features due to its integration with CAD systems. This automated technique can be extended to potentially create multi-material heterogeneous cell constructs.

An experimental setup was designed for photo-patterning of polyethylene glycol diacrylate (PEGDA) hydrogels as shown in Figure 3.1. The main components of the setup include a UV light source (Cure SpotTM 50), UV Fused Silica Planoconvex collimating lenses (f =50 mm, Newport, CA), 365 nm filter (Edmund Optics, NJ), Texas Instruments DMD, projection lens (f = 25 mm, Newport, CA) and a mold to contain the pre-polymer solution. The function and working of the DMD^{TM} have been detailed by Lu et al (2006) and Sun et al (2005), to which the readers can refer for further information on setup and functioning. Yasar et al (2009) also have briefly outlined the set-up and the process of transferring L-system-based designs to the DMD^{TM} chip system.
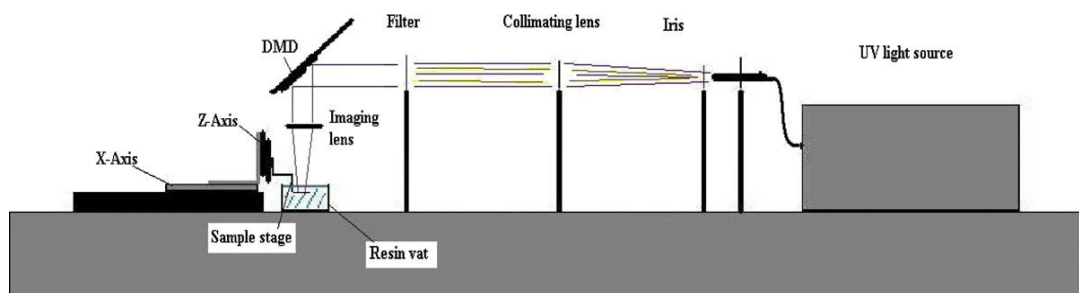
Figure 3.1 Schematic of the maskless DLP^{TM} photolithography process.

Photopolymerization is enabled by the UV light source which is collimated through the configuration of lenses and reflected off the DMD mirror placed at 45∘ onto the resin vat. The DMD memory chip contains aluminum micro-mirrors which can be individually tilted either −10∘ or +10∘. When a micro-mirror is tilted +10∘ it is considered to be in the 'on' mode, and likewise when a micro-mirror is tilted −10∘, it is considered to be in the 'off' mode. Illumination from the UV light source reflects on the

38

resin vat only when the micro-mirror is in the 'on' mode, while 'off' mode pixels appear dark. The 'on' mode for each micro-mirror is directed by the bitmap image loaded to the chip system. Each white pixel on a .bmp image represents the 'on' state of the micro-mirror, while a black pixel corresponds to an 'off' state of the micromirror. Thus, the bitmaps instruct the mirrors to selectively pass UV light based on their on/off modes.
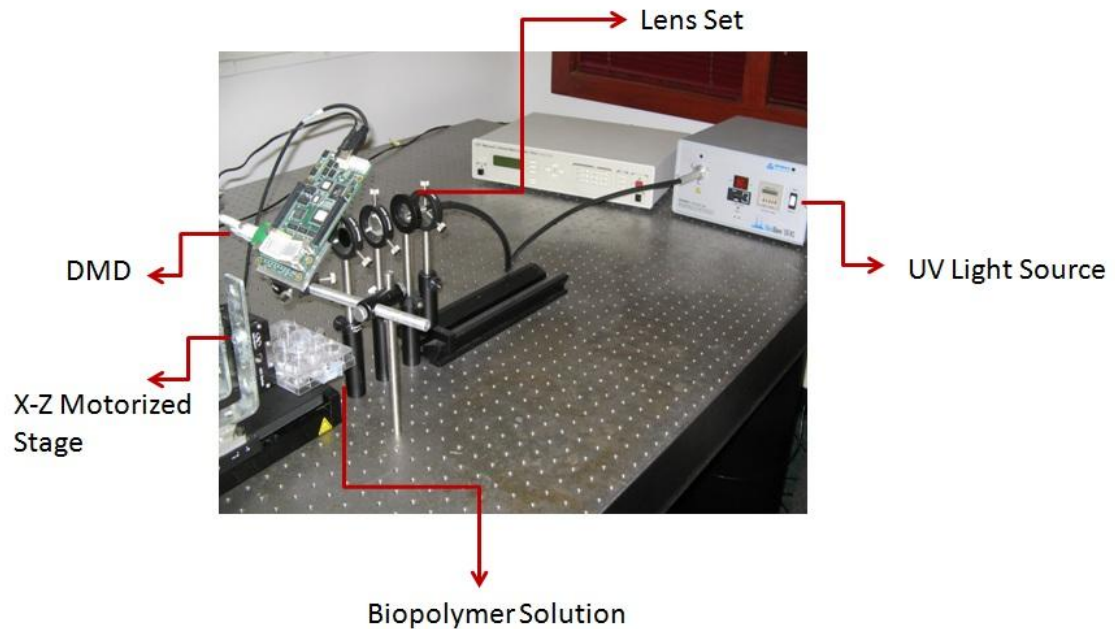
Figure 3.2 Picture of Digital Micro-mirror Device photolithography set-up.

3.2 Fabrication of PEGDA Hydrogels Using DLP Based Maskless Photolithography
3.2.1 Hydrogel Chemistry

As described in Arcaute et al's paper (2006) Poly(ethylene glycol) diacrylate (PEGDA) is highly biocompatible material and it has widely used biological applications. Christopher et al (2011) claims that PEGDA based hydrogel scaffolds

permit great biological and biomechanical customization. Liu et al (2002) also explained that PEG based hydrogels are biocompatible. These types of hydrogels have been used to homogenously immobilize various cell types including chondrocytes Bryant et al (2002), Ellisseeff et al (2000); vascular smooth muscle cells Mann et al (2001); and fibroblast Gobin et al (2002) and Hern et al (1998). In our study PEGDA (3.3kDa) was dissolved in distilled water to form 20%, 50% and 80% v/v solution. On the other hand, to start the polymerization chain through the fabrication process, 0.50gr of photoinitiator 2,2-dimethoxy-2-phenyl-acetophenone was dissolved in 1mL of solvent of 1-vinyl-2-pyrrolidinone. After that the solution of 0.50mg/mL of 2,2-dimethoxy-2-phenyl-acetophenone in 1-vinyl-2-pyrrolidinone was added to PEGDA-water mixture in concentrations of 0.6mg/mL, 0.7mg/mL and 0.8mg/mL. The final solution was kept in a dark environment to prevent the crosslinking process.

3.2.2 Layered Scaffold Fabrication with Maskless Photolithography

In our research the files generated in the computer environment and they are converted to points and loaded into an AutoCAD environment. The points were processed to obtain bitmap images of the resulting structure. If a 2D branched network is designed, the algorithm outputs a bitmap image of the L-system design. In a 3D based L-system model, a slicing procedure can be utilized to obtain the bitmap images at each slice level location. The height of the imaging lens is adjusted to focus the projected image onto the top surface of the pre-polymer. Upon UV exposure (365 nm, 5 mW cm−2), the pre-polymer solution crosslinks to produce the first hydrogel layer. Successive layers can be produced by lowering the stage, similar to that of a

stereolithography system. Care is taken not to disturb the hydrogel during the material addition process. The time of exposure for each layer is controlled to ensure proper bonding between the layers. After fabrication, the gels are washed to remove any uncrosslinked solution and placed in an aqueous solution. Unlike a stereolithographic system, curing takes place instantaneously with the reaction kinetics taking place within 50s. As explained by Yasar et al (2009) the time of exposure can however be controlled by the level of photoinitiator concentration and level of PEGDA concentration present in the prepolymer solution.

Figure 3.3 Representation of Digital Micro-mirror Device. The middle row shows the "on" mode micro-mirrors.

Figure 3.3 represents how white micro-mirrors which are shown with the bitmap image of "one"s reflect the UV light to the prepolymer solution and start the polymerization chain to produce the hydrogels. Likewise the black micro-mirrors reflect the UV light away from the prepolymer solution and keep the non-illuminated area remain in the liquid form.

Our experimental results proved that "DLP^{TM} based Maskless Photolithography" has noticeable advantages compared to other fabrication techniques. First of all since

the scaffolds can be fabricated in layer by layer fashion, interior architecture of the fabricated scaffolds can easily be controlled with this fabrication method. Vozzi et al (2003) also emphasis that scaffolds with a well-defined internal geometry at micron scale enables the study of cellular activity to lead the development of engineered tissues. Moreover there is no need to use expensive fabrication mask. The masks can be designed in the computer environment and loaded to digital micro-mirror device to generate the different shape scaffold layers. In addition to that UV light with the wavelength of 365nm enables the cell encapsulation. Cell encapsulation experiments can be done with this range of UV wavelength. Another advantage of using maskless photolithography technique is, any biocompatible and photopolymerizable polymers and copolymers can be used as a biomaterial to start the polymer chain after the interaction with UV light. Lu et al (2005) emphasis that in order to achieve degradable scaffold structures, enzymatically or hydrolytically degradable moieties, as reported by Anseth and colleagues (2002), Davis et al (2002), Metters et al (1999) or Hubbell and colleagues (2002) could also be used in the DMD based photolithography system. When it comes to the fabrication time, it takes less than a minute to fabricate the layers. In stereolithography fabrication process UV light moves over the biopolymer and illuminated area gets solidified. However, in photolithography process hydrogel parts are being produces in one single UV light shot. In other words, photolithography is much faster than stereolithography. Figure 3.4 shows the schematic comparison of photolithography with stereolithography. Another advantage of using maskless photolithography is any complex shapes can be photopolymerized with the use of

bitmap slices. Table 3.1 summarizes the advantages of maskless photolithography fabrication technique.

Figure 3.4 (a) Schematic representation of streolithography. UV light move over the biopolymer and generate the hydrogels. (b) Schematic representation of photolithography. Hydrogels are produced in one single UV light shot.
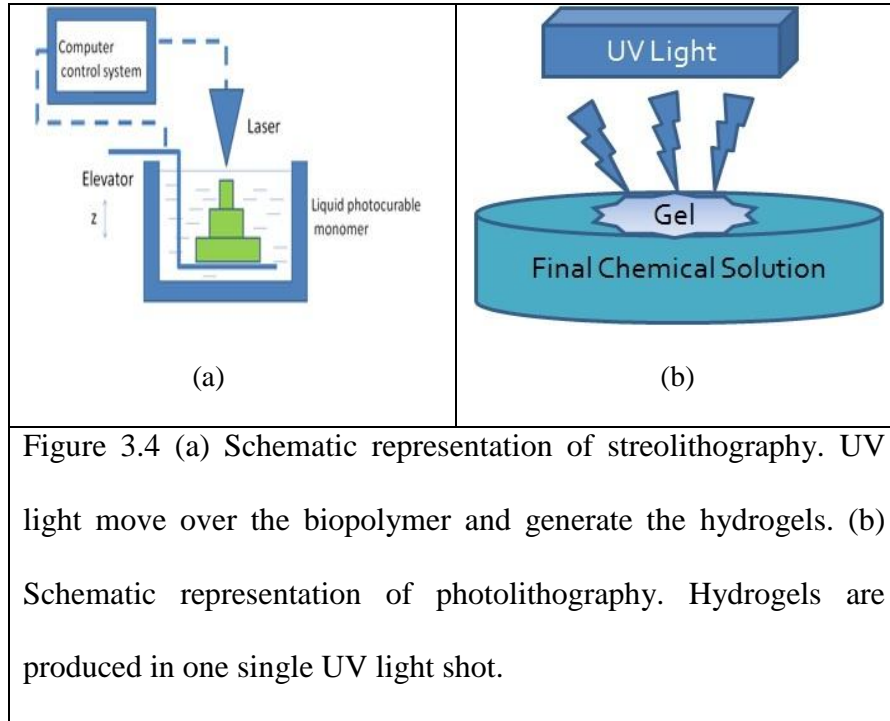
Table 3.1 Summary of advantages of Maskless Photolithography Fabrication Technique

Advantages of DLP^{TM} Based Maskless Photolithography
No Use of Expensive Masks
UV Light at 365nm enables the cell encapsulation
Any biocompatible and photopolymerizable polymers or copolymers can be used
Fast compared to Streolithography
Complex shapes can be photopolymerized with the use of bitmap images

Although maskless photolithography has advantages over the other fabrication techniques it has some limitations too. For instance it is a big challenge to do deposition

43

of multiple biomaterials precisely. The wavelength of the UV light used for the maskless photolithography is as explained earlier 365nm. According to Lu et al (2006) this wavelength does not really kill the cells. However, it might have some harmful effects for cells. Lu et al (2006) stated that UV exposure time can always be reduced by increasing the UV light intensity, increasing the concentration of photoinitiator or increasing the concentration biopolymer. The disadvantage of increasing the light intensity causes to have worse scaffold resolution. Tissue engineering research also showed that some photoinitiators have also harmful effects in cell encapsulation process. Valeria Liu and Sangeeta Bhatia (2002) proved that the photoinitiator methoxy-2-phenyl-acetophenone has toxic effects for the HepG2 cells at amounts greater than 0.9mg/mL. The limitations of the maskless photolithography technique is listed in Table 3.2

Table 3.2 Summary of limitations of Maskless Photolithography Fabrication Technique

Limitations of DLP^{TM} Based Maskless Photolithography
Precise deposition of multiple biomaterials is difficult
Effects of UV Light on cells
Use of harmful photo-initiators in case of cell encapsulation procedures

Figure 3.5 demonstrate the different shapes of hydrogel scaffolds obtained with maskless photolithography.

Figure 3.5 Different shape of single layer PEGDA based hydrogels obtained with maskless photolithography
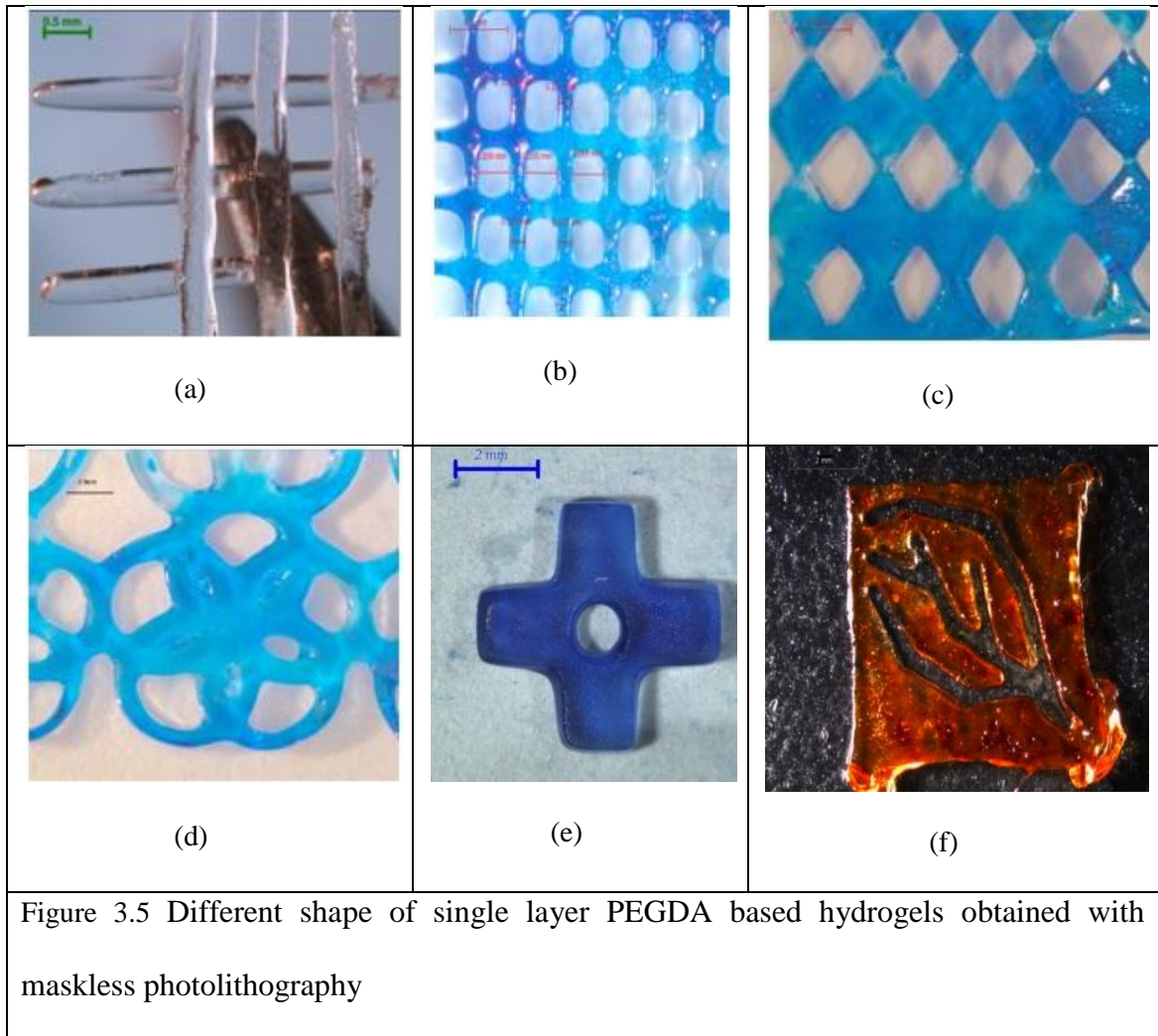
This system is also capable of fabricating complex shape layered structures. Also each layer can be designed and fabricated separately to control the internal micro-architecture of the thick scaffolds. As shown in Starly et al's (2006), Langer et al's (1993), Zeltinger et al's (2001) and Hutmacher et al's (2001) papers The tissue scaffold micro-architecture is believed to influence the behavior of cells and the biological function of tissues by providing a nutritional pathway as well as a spatial distribution for cell growth and proliferation.

Figure 3.6 (a) (b) Single layer obtained by maskless photolithography system (b) Two layered structure, each layer thickness is 150µm   (c) Multi-layered structure, a ring crosslinked over a patterned layer
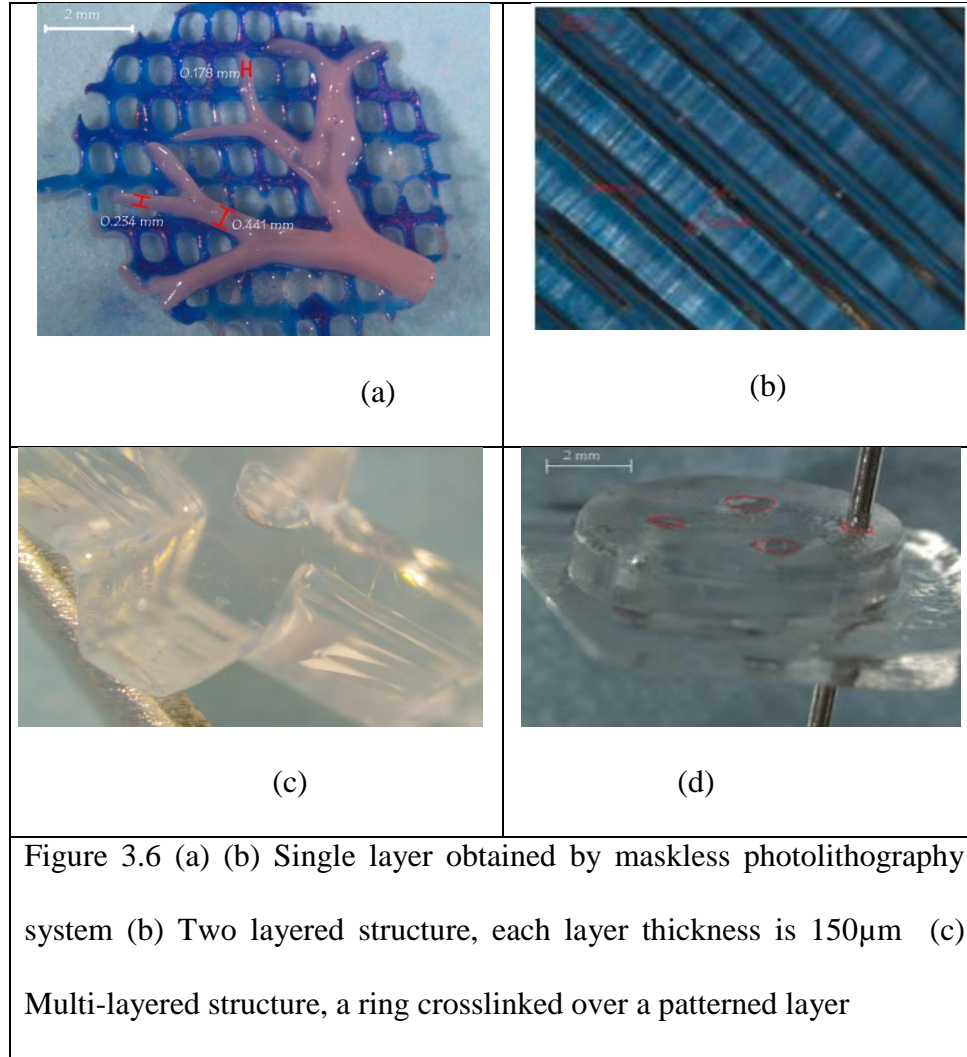
In this method as explained earlier photopolymerization is enabled as a result of the interaction of UV light and photopolymerizable biomaterial. Figure 3.7 gives an idea about the fabrication of two layers of PEGDA hydrogels. Lu et al (2006) emphasis that in order to produce the first layer, the solid line was designed and conveyed to the DMD to let the polymer cure and create the solid gels only at the point where it is selectively exposed by UV laser light. Once the first layer was produced three sequential squares were designed and sent to the DMD to construct the second layer on

the top of first layer. Likewise more successful layers can be obtained by adding the fresh solution to the hydrogel and repeating the similar curing process. In addition to that curing takes place instantaneously with reaction kinetics taking place within seconds and this novel feature brings more advantage to the maskless photopolymerization compared to streolithographic systems.
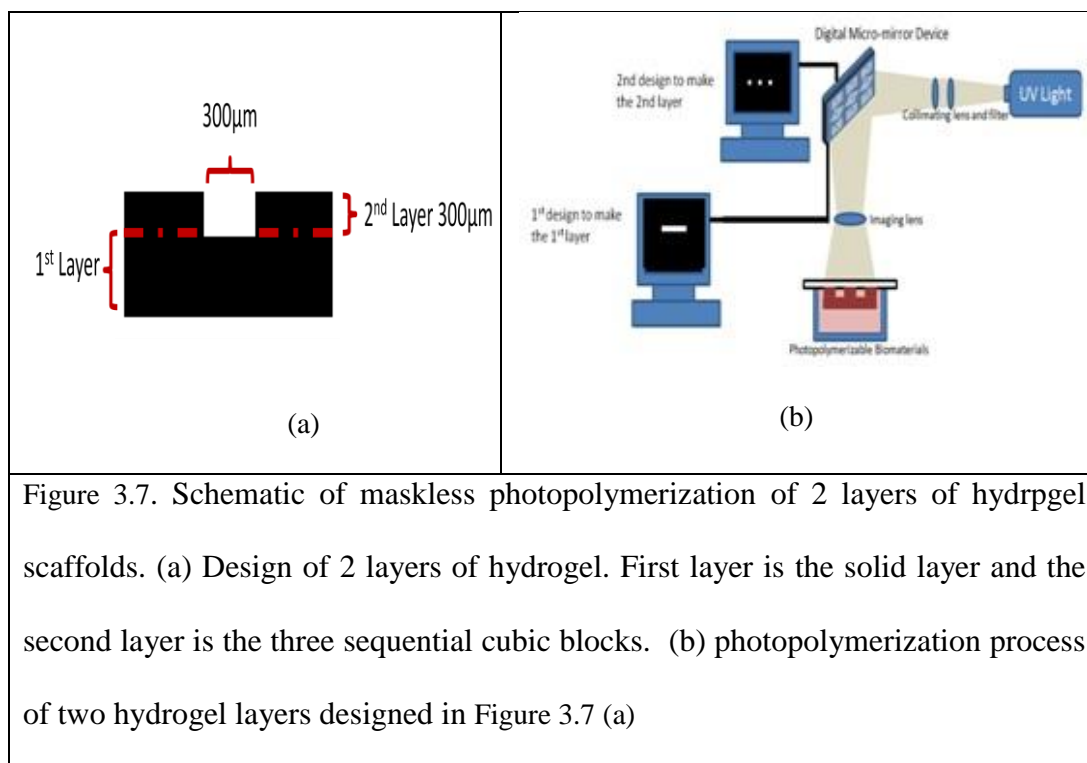
Figure 3.7. Schematic of maskless photopolymerization of 2 layers of hydrpgel scaffolds. (a) Design of 2 layers of hydrogel. First layer is the solid layer and the second layer is the three sequential cubic blocks. (b) photopolymerization process of two hydrogel layers designed in Figure 3.7 (a)

As a result of 2 layers of fabrication process explained in Figure 3.8 the following hydrogels were obtained.

Figure 3.8 Some of the fabrication results for the design shown in Figure 3.7
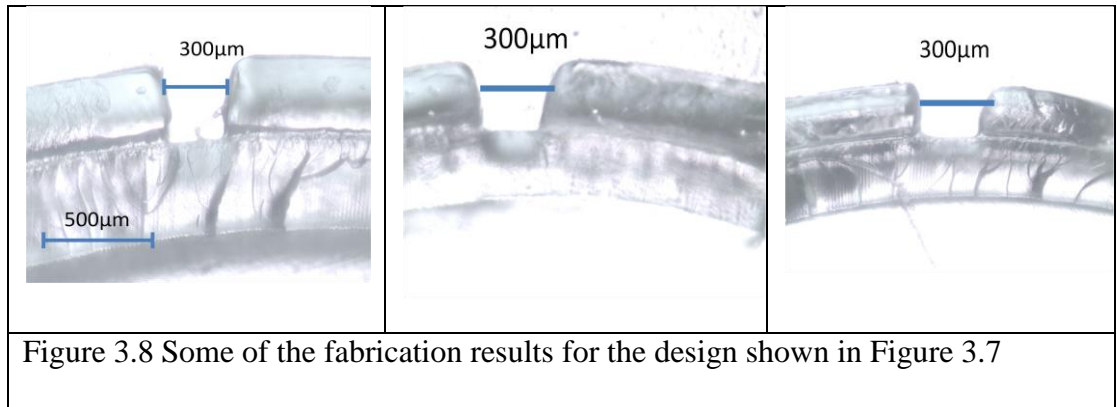
We have conducted our first part of scaffold design with the fabrication process. Figure 3.9 shows the 3D structures fabricated with 50% PEGDA that was designed as shown in Figure 2.11 a, Figure 2.11 b and Figure 3.10. These fabricated parts consist of 3 layers. First layer is a solid layer and it is crosslinked by UV light for 65 seconds. The second layer has y-shape micro-fluid channels on it and UV exposure time was chosen 25 seconds to form the second layer at the top of the first layer. Once first two layers were obtained it is washed with water to remove the uncrosslinked polymer solution from the microchannels. As Starly et al (2006) suggested, after first two is rinsed, the third layer was crosslinked in 20 seconds as a solid layer which has the same features with the first layer. In other words the y-shape is sandwiched between two solid layers and these channels are empty channels to provide the nutrient flow for interior of the scaffold. During the fabrication process UV light intensity was kept constant and uniform.

48

Figure 3.9. (a)-(b)-(c)-(d) Illustrate the three layers scaffolds. Micro-channels sandwiched between two solid layers. (a)-(b)-(c) fabricated according to L-system formulations given in Figure 2.11 a

(d) fabricated according to L-system design given in Figure 2.11 c. (e) fabricated according to the L-system design shown in Figure 3.10 b (f) side view of the two layers of PEGDA hydrogel

49

```
#define STEPS 3    #define a_1 65   #define a_2 -65

 #define a_3 0       #define phi_1 0     #define phi_2 0

#define r1 0.65      #define r2 0.65  #define q 0.5

 #define e 0.5     #define k 0.5        #define omega_0 0.8

#define min 0.1    Lsystem: 1     derivation length: STEPS

Axiom:?E(0,0)?P(0,0)A(8,omega_0)B(8,omega_0)

      C(8,omega_0)D(8,omega_0)

A(s,w): s >= min--> !(w);(255)F(s) [+(a_1)/(phi_1)A(s*r1,w*q^e)]

    [+(a_2)/(phi_2)A(s*r2,w*(1-q)^e)]

B(s,w): s >= min  -->  !(w);(255)|F(s/2)-(90)F(s)

C(s,w): s >= min  -->  !(w);(255)|F(s)+(0)F(s)

D(s,w): s >= min  -->  !(w);(255)|F(s)-(270)F(s/2)

                [+(a_1)/(phi_1)A(s*r1,w*q^e)]

              [+(a_2)/(phi_2)A(s*r2,w*(1-q)^e)]

Endlsystem
```


Figure 3.10.   (a) L-System mathematical formalization to produce Figure 3.10. (b) Vascularization system design obtained with the L-System formulization given in Figure 3.10 (a)

3.3. Effect of Maskless Photolithography Parameters on Hydrogel Accuracy

As explained in Khalil et al's paper (2005) a fabrication method that maintains a high level of accuracy is necessary to maintain the consistency and repeatability in accordance to the initial design. The Digital Micromirror Device has the capability of producing precise and spatially designed micro level patterns. The quality and the accuracy of the fabricated particles strongly depend on the UV exposure time, concentration of the biopolymer and concentration of the photoinitiator. The role of the optical device setup is to provide the uniform and proper UV light distribution on the surface of the biopolymer solution.

Since the choice of scaffolds plays an important role to enable the cells to behave in the required manner to produce desired shape and size tissues, scaffold fabrication needs to be developed in an appropriate way to generate high accuracy by using the right fabrication parameters such as UV exposure time per layer, concentration of photoinitiator, concentration of PEG and intensity of the UV light. Wrong choice of these parameters causes either over-crosslink or under-crosslink scaffolds as shown in Figure 3.12.
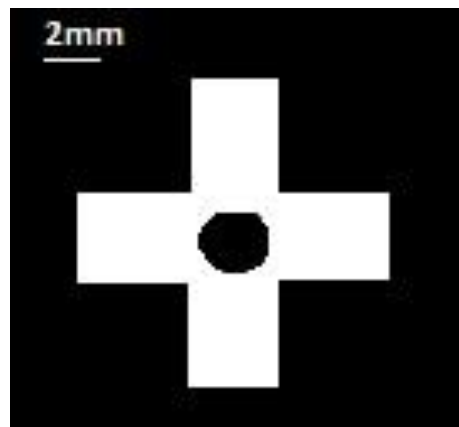
Figure 3.11 Bitmap image of a cross with a hole

Figure 3.12 (a) shows the most accurate fabricated cross shape hydrogel. First of all the cross shape with a hole inside was designed in the computer environment as seen in Figure 3.11 and then it is loaded to digital micro-mirror device. In order to obtain Figure 3.12 (a) UV light sent to the biopolymerizable solution for 20 seconds. The cross shown in Figure 3.12 (b) was obtained in the same conditions except the UV exposure time was increased from 20 seconds to 25 seconds. An over-crosslinked hydrogel obtained due to higher UV exposure time. As it can be clearly seen in Figure 3.12 (b),

after the 25 seconds of fabrication process the hole in the middle of the cross was blocked and the edges of the cross became extremely bigger than what it is supposed to be. Our experiment results also showed that under-crosslinked hydrogels occurs when using the less UV exposure time than the required UV exposure time which were determined by experiments Figure 3.12 (c) shows the hydrogel which was obtained in 15 seconds. As a result of under-crosslinked hydrogel, the leg of the cross occurred thinner than that of the bitmap image, as shown in Figure 3.11. Also diameter of the hole inside the under cross shown in Figure 3.12 (c) obtained bigger than that of the bitmap image in Figure 3.11.

| (a) | (b) | (c) |

Figure 3.12. (a) Illustrates hydrogel part with appropriate parameters: exposure time, concentration of PEG and concentration of photoinitiator. (b) over-crosslinked hydrogel. (c) under-crosslinked hydrogel
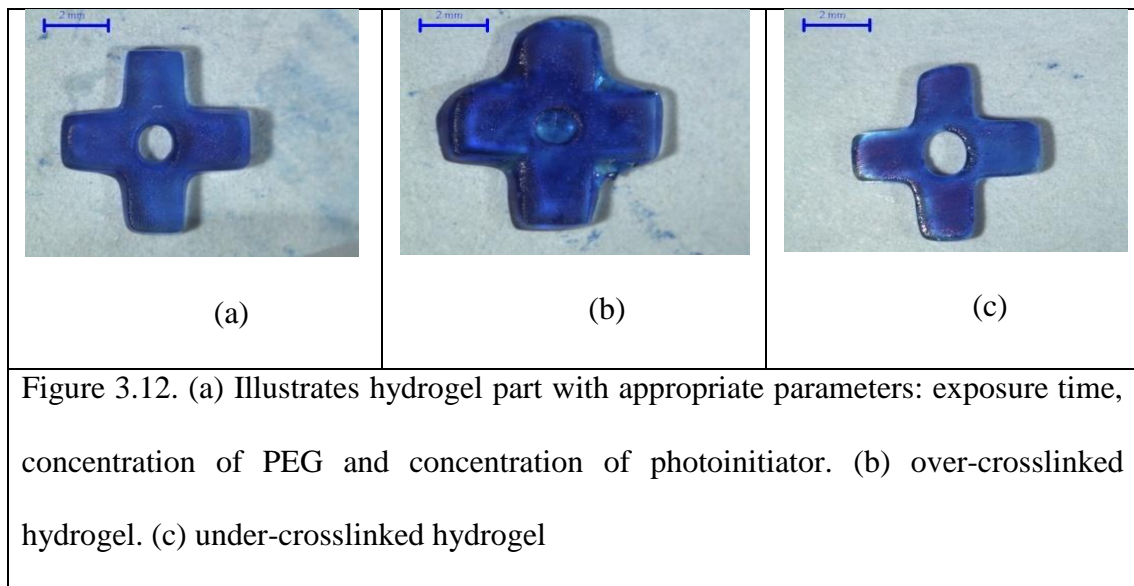
In most cases to fabricate the tissue engineered scaffolds low intensity UV light is needed to achieve the success in cell encapsulation. In photolithography process UV light intensity can always be reduced by increasing the either UV exposure time, concentration of polymer or concentration of photoinitiator. However changing each of these photolithography parameters affects the obtained hydrogel accuracy. In order to

generate the hydrogel layers with high accuracy photolithography parameters should be precisely chosen. In this work influence of UV exposure time, concentration of PEGDA and concentration of photoinitiator on hydrogel accuracy was investigated. First of all bitmap image of a rectangular prism and a second layer with a single channel were designed as shown in Figure 3.13 a.

Figure 3.13 (a) Design of layer thickness study (b) PEGDA samples produced by according to the design shown in Figure 3.13 (a)
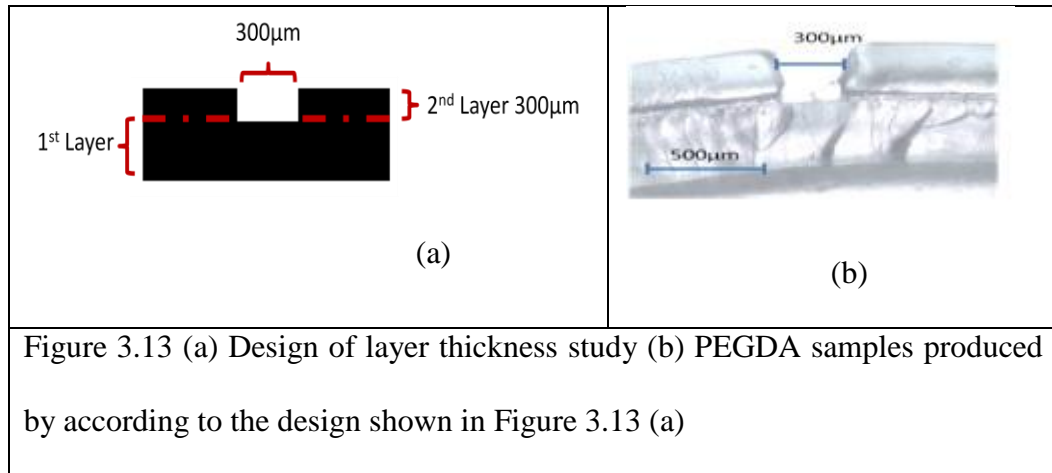
In order to generate the second layer with 300µm thickness the desired PEGDA solution is 60µl. In order to investigate the influence of the photolithography parameters three sets of PEGDA solutions 20%, 50% and 80%PEGDA were prepared. The photoinitiator concentrations were chosen 0.6mg/ml, 0.7mg/ml, 0.8mg/ml. The UV exposure time was chosen 11sec, 13sec and 15sec. For every combination of PEGDA concentration, photoinitiator concentration and UV exposure time the designed micro-channel shown in Figure 3.13 a was fabricated. After that the second layer thickness was measured with Leica microscope and the data were analyzed with software Design-Expert 8.0.4 to generate the ANOVA test table. According to ANOVA table the model F-value of 12.78 implies the model is significant. There is only a 0.01% chance that a

"Model F-Value" could occur due to the noise. Values of "Probability > F" less than 0.05 indicate model terms are significant. Our results also prove that choosing the right experimental parameters have significant influence of process accuracy and hydrogel reproducibility. According to Design-Expert 8.0.4 the final thickness of a hydrogel can be calculated in terms of actual factors with the following formulation

Layer thickness = 0.23 + 0.025 *(UV Exposure Time) + 0.050*(PEGDA Concentration) + 0.043*(Photoinitiator Concentration) - 3.25E-03*(UV Exposure Time)*(PEGDA Concentration)-7E-03*(UV Exposure Time)* (Photoinitiator Concentration)-0.036*(PEGDA Concentration) *(Photoinitiator Concentration)   (6)

This formulization gives the information about required UV exposure time to cure the given concentration of PEGDA and photoinitiator to obtain a fixed thickness.

(a)   (b)   (c)
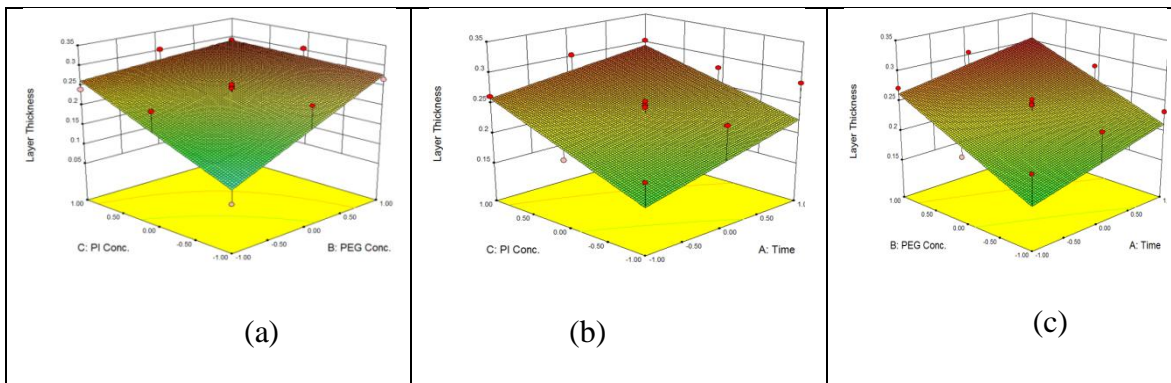
Figure 3.14 3D surface plots. Influence of UV exposure time, concentration of PEGDA and concentration of photoinitiator on hydrogel layer thickness

54

Table 3.3 Analyses of Variance Table

Source	Sum of Squares	Df	Mean Square	F-value	P-value Prob>F	
Model	0.11	6	0.018	12.78	<0.0001	Significant
A-Time	0.011	1	0.011	7.99	0.0091	
B-PEGDA Concentration	0.046	1	0.046	33.04	<0.0001	
C-PI Concentration	0.033	1	0.033	23.56	<0.0001	
AB	1.268E-004	1	1.268E-004	0.092	0.7646	
AC	5.880E-004	1	5.880E-004	0.43	0.5204	
BC	0.016	1	0.016	11.56	0.0023	

Our experiments also proved that if the fabrication parameters are chosen less than what they should be to produce the actual size and shape scaffolds as designed with bitmap images then the second layers occur under-crosslinked. Figure 3.15 shows that how the channels located into the second layer under-crosslinked and did not form completely due to the chosen fabrication parameters.

Figure 3.15 Under-crosslinked two layers of PEGDA based hydrogels
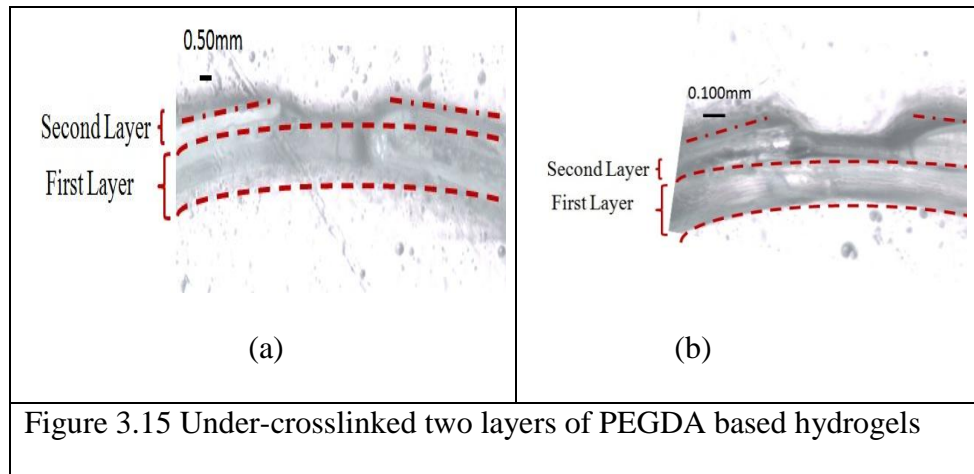
Likewise if the fabrication parameters are chosen more than what they should be to produce the actual size and shape scaffolds as designed with bitmap images then the second layers occur over-crosslinked. Figure 3.16 shows that how the channels located into the second layer over-crosslinked and the channels were blocked.

0.300mm

Second Layer

First Layer

(a)

0.300mm

Second Layer

First Layer

(b)
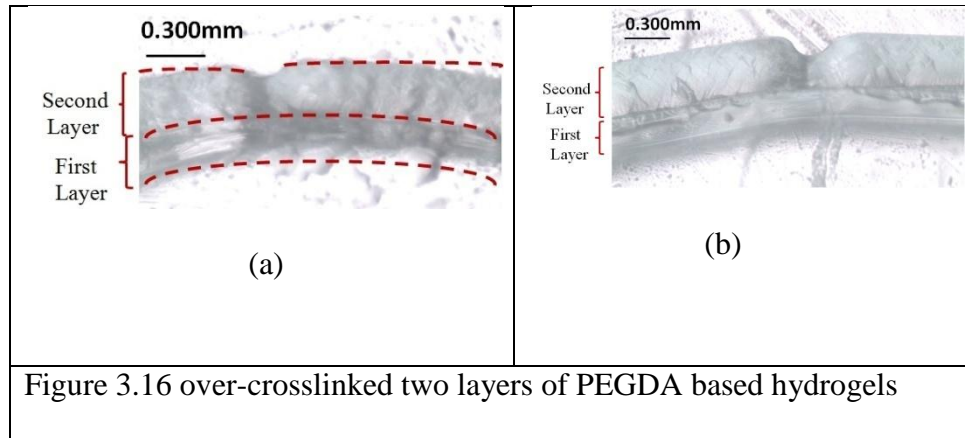
Figure 3.16 over-crosslinked two layers of PEGDA based hydrogels

Kim et al (1998) and Gecgil et al (2010) studied that successful construction of healthy tissues relies on the structural environment. Therefore scaffolds must carry spatial properties such as the right porosity and mechanical strength to mimic the vasculature networks present in the human body. This step only can be achieved with the precise internal architecture control of the fabricated scaffolds. Thus in our research we also run the experiments to see what the smallest level of layer thickness we can obtain and our experiment results indicate that we can easily produce the scaffold layers as small as 30μm as shown in Figure 3.17.
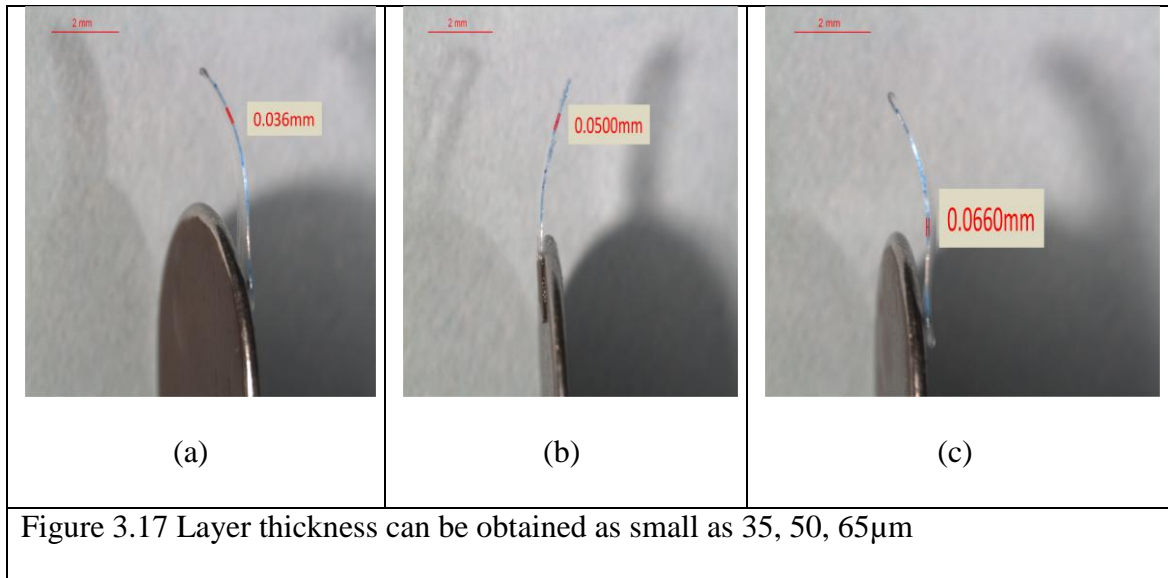
Figure 3.17 Layer thickness can be obtained as small as 35, 50, 65µm

3.3.1. Channel Characterization

The effects of PEGDA concentration and Photoinitiator concentration on hydrogel patterning accuracy were investigating with the design and fabrication of the patterns shown in Figure 3.13. A well with a 300µm width, 300µm length and 300µm thickness was designed and fabricated as explained in detail in the previous section. Our experimental studies showed that due to the light diffraction visible imprecise edges were occurred during the fabrication process. First of all 20%, 50% and 80% PEGDA solutions with 0.5mg/ml, 1mg/ml and 1.5mg/ml photoinitiator concentrations were prepared and for all combination of PEGDA and photoinitiator concentration two layers of hydrogel patterns shown in Figure 3.13 a was fabricated. After the fabrication process the side view of the hydrogels were taken with Leica microscope and recorded to do the comparison of the ideal wells with the fabricated hydrogel wells. Area covered by the hydrogel well was measured by a MATLAB code using the image pixels. The measured data was compared with original bmp image which was designed and used for the fabrication process like Chu et al (2007) did.

57
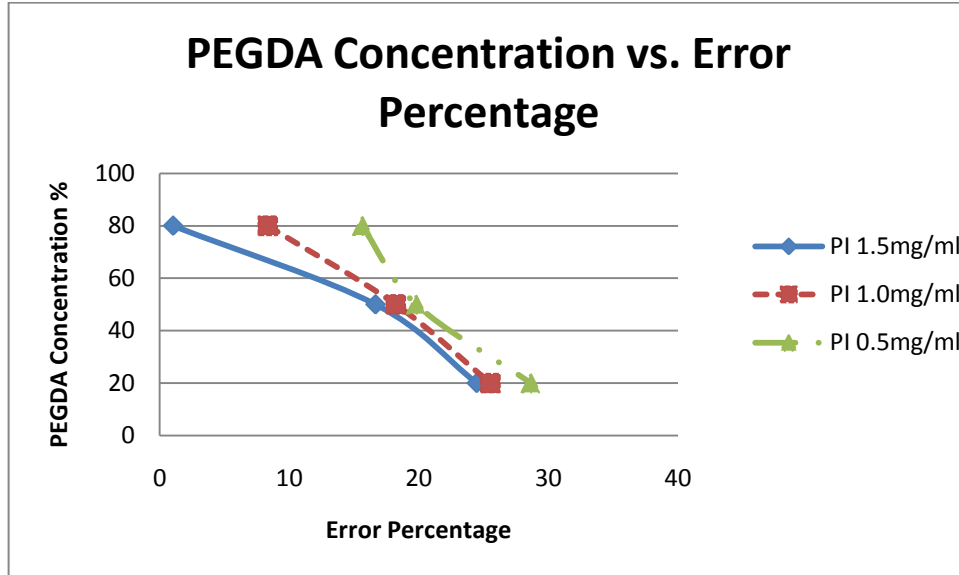
Figure 3.18 Effect of PEGDA concentrations on fabricated hydrogel accuracy.

Figure 3.18 describes higher concentration of PEGDA and higher concentration of photoinitiator generates more accurate hydrogel. As shown in Figure 3.19 a for the 80% PEGDA and 1.5mg/ml photoinitiator concentration the most ideal pattern was achieved. Likewise for the 20% PEGDA and 0.5 mg/ml photoinitiator concentration the biggest imprecise well edges occurred and this is also shown in Figure 3.19 b
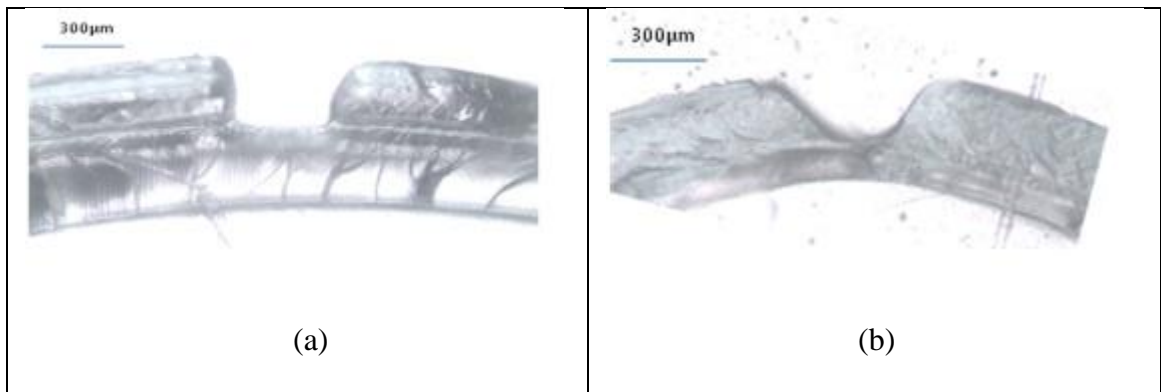
Figure 3.19 Examples of multilayer structures for the investigation of photolithography parameters on hydrogel accuracy. (a) most ideal pattern obtained with 80% PEGDA and 1.5mg/ml photinitiator (b) the biggest imprecise well edges obtained with 20% PEGDA and 0.5 mg/ml photoinitiator

Some other results that we obtained were shown in Figure 3.20. Patterned hydrogels were obtained with 50% PEGDA. UV exposure time was 20 seconds for the first layer and 10 seconds for the second layer. Channel width and thicknesses are varying from 200µm to 350 µm. After the fabrication process, blue color fluid run through the channel to show that channel is not blocked during the fabrication process and the top view of hydrogel's picture which is shown in Figure 3.20 a, b and c. These pictures were taken with the microscope Leica. After that in order to show the desired layer thickness was achieved and also the channel is actually open, the hydrogel was tilted and it is cut as shown in Figure 3.21.

(a)	(b)	(c)
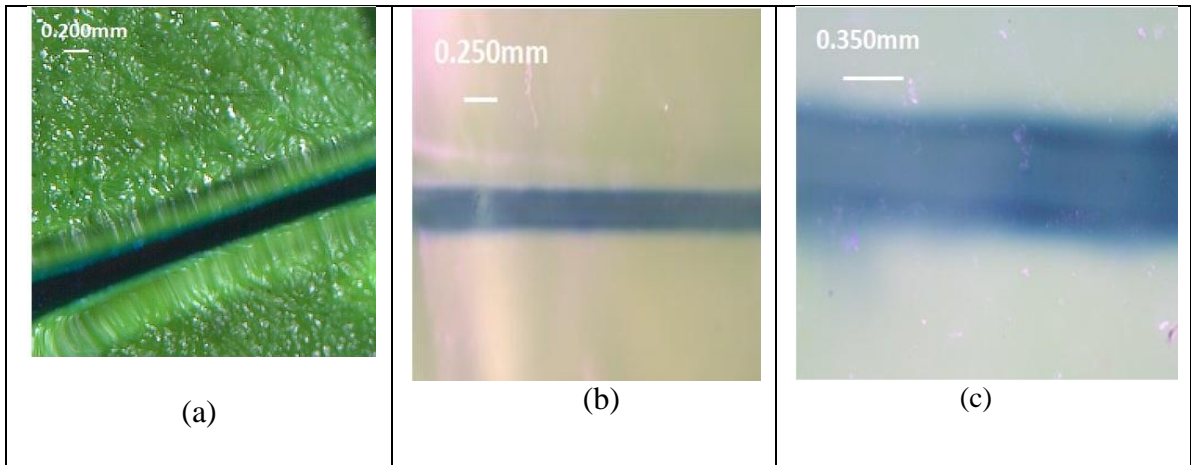
Figure 3.20 Top view of hydrogels with the channels. The widths of the channels are 200μm, 250μm and 350μm respectively.

(a)	(b)	(c)
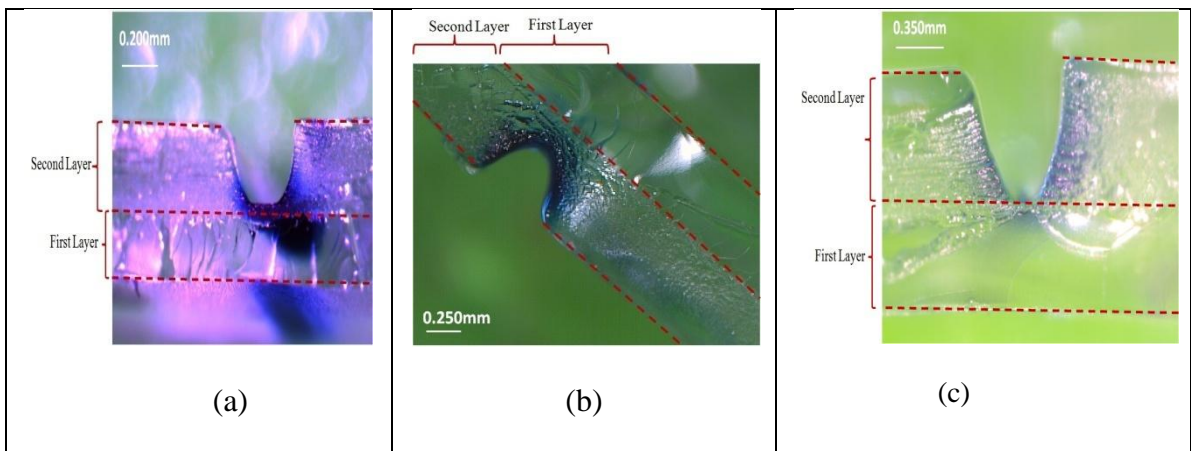
Figure 3.21 Side view with two layers of crosslinked hydrogel. The thickness of the channels are 200μm, 250μm and 350μm

Figure 3.21 proves that after the maskless photopolymerization process, the channels are still open, they can serve as nutrient and oxygen flow channels for cells which are located at the interior of the scaffolds.

3.4. Conclusion

Recent works done in tissue engineering show that researchers have been focusing on manufacturing methods such as soft lithography, photolithography and solid freeform fabrications.

Until recently, most of these techniques had limited capability in producing three-dimensional scaffolds because the lack of ability of nutrient and oxygen access to deep into the scaffolds. Because of this reason the cells located at the interior of the scaffolds couldn't get sufficient nutrient and died out. In order to handle this problem, as explained in detail in the previous chapter first of all L-Systems were used to generate the vascularization networks to provide the sufficient nutrients and oxygen for cells to survive. After this step, DLP based maskless photolithography was used to fabricate the scaffolds in layer by layer fashion. Some of the main reasons why maskless photolithography was chosen for the fabrication process can be summarized as the following:

- Maskless photolithography doesn't require using expensive masks.
- One of the maskless photolithography fabrication components is UV light with the wavelength of 365nm and wavelength of 365nm is not harmful for the cells and it enables the cell encapsulation
- Any biocompatible and any photopolymerizable polymers or copolymers can be used to generate the scaffolds
- Maskless Photolithography is faster than streolithography. In streolithography process, UV light moves over the polymer solution to generate the parts whereas

the same shape parts can be generated in one UV exposure shot in maskless photolithography

- Any complex shapes can be photopolymerized with the use of bitmap slices.

Basically maskless photolithography refers to the process of photolithography without the use of physical masks. Patterning is achieved using the DLP^{TM} technology of Texas Instruments. Maskless photolithography has five major components. These components are:

- UV Light Source (365nm, 25mW/cm^2)

- Collimating and Imagining Lens Set

- DMD Chipset

- X & Z Motorized Stages

- Photopolymerizable Biomaterials

Layers are designed separately in the AutoCAD environment and they are loaded to DMD. The hearth of the fabrication setup is DMD Chipset. It consists of hundreds of tiny micro-mirrors. Each of these tiny micro-mirrors can be controlled and tilted either towards to the UV light source or away from the UV light source individually. The micro-mirrors which face the UV light source are called "on" mode and they reflect the UV light to the photopolymerizable biomaterial. Other micro-mirrors don't reflect the UV light to the photopolymerizable solution. In other words the designed layer shape is loaded to DMD, and UV light reflects the designed shape to the biocompatible polymer. When UV light interacts with the photopolymerizable biomaterial, the illuminated area gets solidified and non-illuminated area stays in the liquid form. This is how first layer of scaffold is produced. Once the successful first

layer is produced, fresh photopolymerizable solution is added over the first layer and same procedure is repeated to produce the second layer at the top of the first layer.

In this chapter it is also showed that concentration of PEGDA, concentration of photoinitiator and the UV exposure time has a significant influence on hydrogel accuracy and reproducibility.

The hydrogel thickness formulation is also driven to calculate the required UV exposure time to cure the given concentration of PEGDA and photoinitiator to obtain a fixed thickness. This formulation is given with equation 6 in the third chapter.

Finally we proved that maskless projection photolithography has the capability of producing hydrogels with well-defined, repeatable and complex 3D features due to its integration with CAD systems. This automated technique can be extended to potentially create multi-material heterogeneous cell constructs.

Chapter 4: CELLULAR ENCAPSULATIONS USING DLP BASED

PHOTOLITHOGRAPHY

4.1. HepG2 Cell Encapsulation

The process of engineered tissue begins with the understanding of the basic principles of the cell-cell and cell-environment interaction. Cell-cell interactions were explained in detail by Hamel et al (2002), Napolitano et al (2007) and Dean et al (2007). PEG based hydrogels have been investigated for a variety of tissue engineering applications including cell encapsulation Arcaute et al (2006), Bryant et al (2001), Bryant and Anset et al (2004), Burdick et al (2002), Mann et al (2001) and Williams et al (2003). Although PEG based hydrogels are not bioactive, cell-specific bioactivity can be achieved by trapping the bioactive agents within the hydrogel Arcuate et al (2006), Gunn et al (2005), Mann et al (2002). Mann et al (2001), Mann et al (2001).Success in tissue or organ regeneration can only be achieved if these principles are fully premeditated. In this point our contribution to current research is to investigate the influence of the cell-microenvironment interaction on cell viability.

4.1.1. Cell Maintenance

Cell culture reagents were obtained from Sigma-Aldrich and human liver HepG2 cells were obtained from ATCC (American Type Culture Collection ATTC, Manassas, VA). After HepG2 cells were maintained on Dulbecco's Modified Eagle Medium (DMEM) which was supplemented with 10% fetal bovine serum, 1% penicillin G and streptomycin (Invitrogen) they were incubated at 5% CO_2 and 370C. Cells media was refreshed in every two to three days until the desired cell confluence was

achieved. The cells to be used to form a hydrogel patterns were added to the polymer solution and photoinitiator mixture just before the UV exposure processing.

4.1.2. Preparation of PEGDA Hydrogel Procedure with HepG2 Cells

Once the desired confluence of HepG2 cells were obtained they were tryipsinized by tryipsin/EDTA for 5 minutes and centrifuged at 1500 rpm for another 5 minutes. As a result of spin down procedure in the centrifuge machine HepG2 cell pellet was obtained. On the other hand sterilized Poly(ethylene glycol) diacrylate (PEGDA) (3.3kDa) was dissolved in distilled water to form 50% v/v solution. To start the polymerization chain through the fabrication process, 0.50gr of photoinitiator 2,2-dimethoxy-2-phenyl-acetophenone was dissolved in 1mL of solvent of 1-vinyl-2-pyrrolidinone. After that the solution of 0.50mg/mL of 2,2-dimethoxy-2-phenyl-acetophenone in 1-vinyl-2-pyrrolidinone was added to PEGDA-water mixture in concentrations of 0.6mg/mL. The final solution was mixed with HepG2 pellet. Cells then were exposed with UV light (365nm, 10mW/cm2) for 20 seconds. Once the cell containing scaffolds were fabricated they were kept in the incubator at 370C for an hour.

4.1.3. Cell Viability Kit

Cell viability of the encapsulated HepG2 cells were viewed using Invitrogen live/dead viability kit assay. Once the scaffolds include cells were fabricated the hydrogels were rinsed with water and incubated for one hour with the mixture of 1mL

of PBS, 2μL of ethidium homodimer-1 and 0.5μL of calcein, AM. The fabricated samples then analyzed with the fluorescence microscope.

4.2. Fabrication of Hydrogel Structures Containing HepG2 Cells

Over the past decades, several biomaterial researches and developed different fabrication techniques showed promising results for tissue engineering. However there are some certain challenges still have to be clarified. For instance, in order to treat the critical size defects thick scaffolds must be produced. However lack of accessibility of nutrients and oxygen deep into the scaffolds causes the cell death inside the scaffolds. In order to handle this problem, thick scaffolds must have an inbuilt three-dimensional nutrient distribution network to facilitate the delivery of nutrients for the uniform growth of cells within these man-made matrices until the cells become capable of creating their own vasculature networks. In our research to demonstrate the compatibility of cultured cells with PEGDA based hydrogels we have chosen to use human HepG2 cells because as Enasowa et al (2001) and Rahman et al (2004) reported HepG2 cells are well-characterized immortal cell line with potential applications in bioartificial liver devices. On the other hand since the use of cell friendly and photocrosslinkable PEGDA has a major application role in Tissue Engineering we run our experiments with PEGDA to examine the cell viability. The DMD based maskless photolithography technique was used to fabricate the complex hydrogel based branching networks to provide the nutrient and oxygen flow for HepG2 cells to survive. Firstly, as shown in Figure 2.11 (b) the branching network system was designed with Lindenmayer Systems and it is transmitted to the digital micro-mirror device. Since the

designed branching networks are hollow they are represented with the bitmap image of 1 whereas the surrounding area represented with the bitmap image of 0. As explained in detail in Chapter 4 the tiny micromirrors which represent the "1"s reflects the UV light to the sterilized PEGDA, water and photinitiator mixture. At the same time the micro-mirrors which represent the "0"s reflects the UV light away from the sterilized photocrosslinkable solution. As the UV light hits to the solution it initialize the polymerization chain and illuminated area gets solidified. Figure 4.1 summarizes the fabrication of photocrosslinkable PEGDA with HepG2 cells.
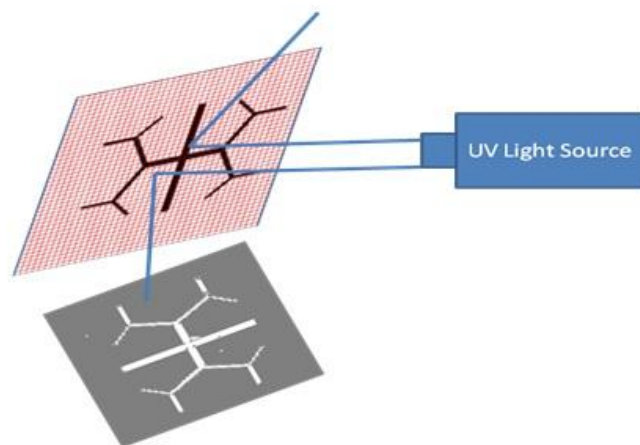
Figure 4.1 Schematic interpretation of PEGDA with HepG2 cells fabrication

After we produced the hydrogels with the maskless photolithography we also investigated the HepG2 cell viability around the branching network channels. After HepG2 cells were used in the fabrication process they attached to the PEGDA solution and they take the branching network form but they don't block the channels. However, these preliminary results indicate that almost all the cells died after the fabrication

process. It might be because of the photoinitiator which is 2,2-dimethoxy-2-phenyl-acetophenone to start curing mechanism. Rago et al (2009), Khalil et al (2001), Chia et al (2000) and Ryan et al (1993) have reported that HepG2 microtissue viability is independent on microtissue size. The future work in this point can be extended to analysis of the photoinitiator effect on cell viability. Different molecular weight of PEGDAs can also be used to figure out what causes the cell death. Figure 4.2 demonstrates the HepG2 cells Live/dead viability.
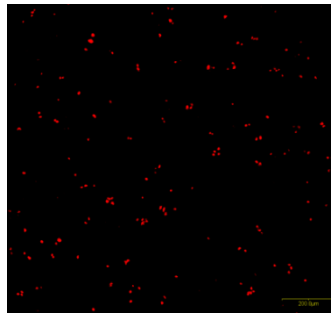
Figure 4.2 HepG2 cell live/dead viability. Fluorescent images of cells after they are exposed with UV light

Chapter 5: CONCLUSIONS AND RECOMMENDATIONS

5.1. Summary

The modeling, design and fabrication of tissue scaffolds to meet multiple biological and biophysical requirements are always a challenge in tissue engineering. This is further amplified when designing load-bearing scaffolds for bone and cartilage tissue applications. In these cases, tissue scaffolds need to be designed with intricate architecture, porosity, pore size and shape, and interconnectivity in order to provide the required structural strength, transport nutrients and the micro-environment for cell and tissue in-growth. By selecting the appropriate unit cell interior structures, properties such as the effective mechanical properties, diffusion and permeability characteristics can be controlled. Depending on the fabrication method used, varying complex internal patterns can be fabricated. In this paper, we have presented the use of Lindenmayer systems in designing vasculature networks that could potentially be incorporated in hydrogel scaffolds. The use of a recursive-based rewriting system provides a powerful method to create complex architecture patterns within the interior of scaffolds. The benefits of using the L-system theory are as follows.

(a) Use of recursive systems to generate complex patterns without the excessive use of CAD graphic resources. The pattern trajectories can be generated in real time and can be implicitly associated with the outer architecture of the scaffold structure prior to manufacturing process plan generation.

(b) Although not described in this thesis, the L-system formulation can be modified to incorporate engineering design constraints into the axiom and rule definition through the use of conditional statements.

(c) The L-system can be parameterized to generate branched networks for specific application depending on nutrition delivery needs. Thus, a single L-system definition can be used to generate several topological networks while maintaining geometry.

(d) STL files need not be generated and can be directly converted to process tool path instructions for fabrication, thus avoiding the bottlenecks of having to convert multi scale models to the triangulated format.

(e) The L-systems can be used to incorporate multiple material definitions within the formulation, hence providing the capability to generate heterogeneous models.

The fabrication process at this stage shows promising results for the capability of producing scaffolds with a complex interior architecture and feature resolution at about 100 μm and larger. The swelling effects of the PEGDA prevent the fabrication of highly repeatable samples below 100 μm. As explained by Northrop et al (1926) and Fialkowski et al (2004) swelling is most likely an inherent property of the hydrogels. This effect can be negated by the addition of other polymer blends into PEGDA such as polylactic acid (PLA) to increase the mechanical strength and biocompatibility of the polymer matrix. Higher resolutions can be obtained by the addition of UV absorbers within the prepolymer solution. Lu et al (2006), Sun et al (2005) and Han et al (2008) showed that UV absorbers prevent the internal reflection of the UV light within the pre-polymer solution.

Since the choice of scaffolds plays an important role to enable the cells to behave in the required manner to produce desired shape and size tissues, scaffold

fabrication needs to be developed in an appropriate way to generate high accuracy by using the right fabrication parameters such as UV exposure time per layer, concentration of photoinitiator, concentration of PEG and intensity of the UV light. These three fabrication parameters also determine the layer thickness. Desired layer thickness can always obtained with the formulation 6.

As it is shown in Underhill et al's work (2007) ff living cells are incorporated within the fabrication process, the amount of water content, photoinitiator concentration, wavelength of UV light will play a role in the viability of the cells .

5.2. Research Contributions

In order to achieve success in tissue engineering, researchers must have the ability of both design and fabrication of tissue scaffolds to help cells to be capable of creating their own vasculature network to form a desired tissue. To design a thick scaffold has been always a challenge for tissue engineers as the chance of accessibility of nutrients deep into the scaffolds becomes less and this causes the cell death. In this thesis we came up with the L-Systems designs to create and control the vascularization system to provide the nutrients and oxygen flow for cells. With the use of L-Systems it is shown that it is possible to design and control complex branching network systems with the L-System axioms, rules and parameters. Second chapter of this thesis explains the influence of axioms, rules and each of L-Systems parameters separately. Each of these parameters determines the angle between the branches, number of the branches, length and width of the branches and the gradual length or width decrees between the

mother and daughter branches. It is also shown that the L-Systems constrains can be built into the L-Systems notations to produce only desired forms of branch structures.

After the development of bio-mimetic design approach of the nutrient and oxygen delivery networks were fully studied, appropriated layered manufacturing system "Maskless Photolithography" was developed. With maskless photolithography polyethylene glycol diacrylate (PEGDA) based scaffolds were produced in varied patterns. In order to control the layer thickness and produce the desired layer thickness scaffolds, the fabrication parameters were investigated and mathematical formulation for the thickness calculation was generated. Moreover the effects of the fabrication parameters on hydrogel accuracy were also studied to form the more accurate hydrogel parts. It is also shown that maskless photolithography technique allows researchers to do cell encapsulation to investigate the cell growth.

5.3. Future Research Recommendations

This work can be improved and can be lead biomedical engineering, material science, molecular biology and biochemistry researchers to make a big contribution for the new cross-disciplinary field of tissue engineering. More specifically, the following research tasks can be considered for the future research development

1. L-Systems definition can be extended to include design and manufacturing constraints into the 3-D branch growth process.

2. An automated multi-material scaffold photopolymerization process can be developed

3. Effect of manufacturing process parameters on the fabrication of living tissue constructs can be studied

4. Concentration of polyethylene glycol diacrylate (PEGDA), molecular weight of PEGDA and concentration of photoinitiator can be tested to examine the cell viability.

5.4. Concluding Remarks

The difficulties, challenges and intricacies of the organ transplantation encouraged engineers and life scientists to work together to find an alternative way to the transplantations of organ. Since the beginning of the 21st century significant research success has been achieved in tissue engineering. However there is still much to be studied and determined to repair the damaged tissue or organ. One of the major successful steps achieved in tissue engineering is the fabrication of the scaffolds to provide the skeleton for cells to attach and grow. However with today's technology the scaffolds thicker than 5mm can't show a success because the cells deep into these man-made matrices die out due to the lack of the sufficient nutrient and oxygen accessibility. In order to address this major problem we suggested to design and fabricate the thick scaffolds with the inbuilt vascularization system to carry the nutrients and oxygen. These vascularization systems weren't generated randomly; they were designed and controlled with the novel rewriting process called L-Systems. L-Systems allow us to control the number of the branches, angle between the branches, length and width of the branches and the gradual length or width decrees between the mother and daughter branches. Once the desired forms of branching structures were designed with L-

Systems, maskless photolithography was used to fabricate the polyethylene glycol diacrylate (PEGDA) based hydrogels. These hydrogels were fabricated in a layer by layer fashion to control the interior architecture of the tissue scaffolds and constructs. Each layer thickness can be adjusted with the control of the fabrication parameters. Researchers who work in this field are now concentrating on how the fabrication parameters effect the cell encapsulation and cell viability. They also work on how to help cells to grow and differentiate into the desired shape of the tissue.

REFERENCES

1. Akiyama. M., Nonomura, H., Kamil S. H., & Ignotz R. A.(2006). Periosteal Cell Pellet Culture System: A New Technique for Bone Engineering. *Cell Transplant* 15, 521.

2. Arcaute, K., Mann, B. K., & Wicker, R. B. (2006). Streolithography of Three-Dimensional Bioactive Poly(Ethylene Glycol) Constructs with Encapsulated Cells. *Annals of Biomedical Engineering*, 34(9) 1429-1441.

3. Atala, A., Bauer, S. B., Dyro, F. M., Shefner, J., Shillito, J., Sathi, S., & Scott, R. M. (1992). Bladder Functional Changes Resulting From Lipomyelomeningocele Repair. *J Urol*, 592-594.

4. Beard, D. A., Bassingthwaighte, J. B. (2000). The Fractal Nature of Myocardial Blood Flow Emerges from a Whole-organ Model of Arterial Network. *J. Vasc. Res.*, 282–296.

5. Bryant, S. J., & Anseth, K.S. (2001). The Effect of Scaffold Thickness on Tissue Engineered Cartilage in Photocrosslinked Poly(ethylene oxide) Hydrogels. *Biomaterials,* 22:619-626.

6. Bryant, S. J., & Anseth, K. S.(2002). Hydrogel Properties Influence ECM Production by Chondrocytes in Poly(ethylene glycol) Hydrogels. *J.Biomed. Res.*, 59(1),63-72.

7. Bryant, S. J., Anseth, K. S., Lee, D. A., & Bader D. L. (2004) Crosslinking Density Influences the Morphology of Chondrocytes Photoencapsulated in PEG Hydrogels During the Application of Compressive Strain. *J.Orthop. Res.*, 22:1143-1149

8. Buijs, J. D., Bajzer, Z., & Ritman, E. L.(2006). Branching Morphology of the Rat Hepatic Portal Vein Tree: A Micro-CT Study. *Annals of Biomedical Engineering,* 34(9), 1420-8.

9. Burdick, J. A., & Anseth, K. S. (2002). Photoencapsulation of Osteoblast in Injectable RGD-Modified PEG Hydrogels for Bone Tissue Engineering. *Biomaterials*, 23:4315-4323.

10. Buckley, C. T., & O'Kelly K. U. (2004). Regular Scaffold Fabrication Techniques for Investigations in Tissue Engineering. *Topics in Biomedical Engineering*, 147-166.

11. Calvert, P., & Liu, Z. (1998). Freeform Fabrication of Hydrogels. *Acta Materialia*, 2565-71.

12. Chia, S. M., Leong, K. M., Li, J., Xu, X., Zeng, K., Er, P. N., Gao, S., & Yu, H.(2000). Hepatocyte Encapsulation for Enhanced Cellular Functions. *Tissue Eng* 6(5), 481-95.

13. Chrobak, K. M., Potter, D. R., & Tien, J. (2006). Formation of Perfused, Functional Microvascular Tubes in Vitro. *Microvasc. Res.,* 71, 185–196.

14. Cabodi, M., Choi, N. W., Gleghorn, J. P., Lee, C. S., Bonassar, L. J., Stroock, A. D. (2005). A microfluid Biomaterial. *J. Am. Chem. Soc.*,127, 13788–13789.

15. David, K. A., & Anseth, K. S. (2002). Controlled Release From Crosslinked Degradable Networks. *Crit Rev Ther Drug Carrier Syst*, 19:385-423.

16. Dean, D. M., Napolitano, A. P., Youssef, J., & Morgan, J.R. (2007). Rods, Tori, and Honeycombs: The Directed Self-assembly of Microtissues With Prescribed Microscale Geometries. *Faseb J*, 21, 4005-4012.

17. De Vos, P., Hamel, A. F., & Tatarkiewicz, K. (2002). Considerations for Successful Transplantation of Encapsulated Pancreatic Islets. *Diabetologia,* 45,159-73.

18. Durst, C. A., Cuchiara, M. P., Mansfield, E. G., West, J. L, Grande-Allen, K. J. (2011). Flexural Characterization of Cell Encapsulated PEGDA Hydrogels with Applications for Tissue Engineered Heart Valves. *Acta Biomater.,* 21329770.

19. Eaglstein, W. H., Falanga, V. (1998). Tissue Egineering and the Development of Apligraf a Human Skin Equivalent. *Advances in wound care : the journal for prevention and healing*, 11(4):1-8.

20. Elisseeff, J., McIntosh, W., Anseth, K., Riley, S., Ragan, P., & Langar, R.(2000). Photoencapsulation of Chondrocytes in Poly(Ethylene Oxide)-Based Semi-Interpenetrating Networks. *Journal of Biomedical Materials Research*, 51(2),164-171.

21. Enosowa, S., Miyashita, T., Fujita, Y., Suzuki, S., Amemiya, H., Omasa, T., Hiramatsu, S., Suga, K., and Matsumara, T. (2001). In vivo estimation of bioartificial liver with recombinant HepG2 cells using pigs with ischemic live failure. *Cell Trans,* 10,429.

22. Folch, A., & Toner, M. (2000). Microengineering of Cellular Interactions. *Annu. Rev. Biomed. Eng*, 02:227–56.

23. Fialkowski, M., Campbell, C. J., Bensemann, I.T., & Grzybowski, B.(2004). Absorption of Water by Thin, Ionic Films of Gelatin. *Langmuir*, 20,3513-3516.

24. Freed, L. E., Guilak, F., Guo, X. E., Gray, M. L., Tranquillo, R., Holmes, J. W., Radisic, M., Sefton, M. V., Kaplan, D., & Vunjak-Novakovic, G. (2006). Advanced tools for tissue engineering: scaffolds, bioreactors, and signaling., 3285–305.

25. Freed, L. E., Vunjak-Novakovic, G.(1998). Culture of Organized Cell Communities. *Adv Drug Delivery Rew*, 33:15-30.

26. Gemmiti, C.V., Guldberg, R.E. (2006). Fluid Flow Increases Type II Collagen Deposit and Tensile Mechanical Properties in Bioreactor-grown Tissue Engineered Cartilage. *Tissue Engineering,* 12, 469–479.

27. Gobin, A. S., & West, J.L.(2002). Cell Migration Through Defined, Synthetic ECM Analogs. *Faseb J.* 16(7),751-753.

28. Golden, A. P., & Tien, J. (2007). Fabrication of Microfluidic Hydrogels Using Molded Gelatin as a Sacrificial Element. *Lab Chip,* 720-725.

29. Gunn, J. W., Turner, S. D., & Mann, N. K. (2005). Adhesive and Mechanical Properties of Hydrogels Influence Neurite Extension. *J. Biomed. Mater. Res.*, 72A(1):91-97.

30. Han, L. H., Mapili, G., Chen, S. C., and Roy, K. (2008). Projection Micro-printing of Three-Dimensional Scaffolds for Tissue Tngineering. *J. Manuf. Sci. Eng.*, 1–4.

31. Hansen, L. K., Hsiao, C. C. H., Friend, J. R., Wu, F. J., Bridge, G. A., Remmel, R. P., Cerra, F.B., & Hu, W. S. (1998). Enhanced Morphology and Function of Hepatocyte Spheroids: A Model for Tissue Self-assembly. *Tissue Eng.*, 4,65.

32. Hern, D.L., & Hubbell, J.L. (1998). Incorporation of Adhesion Peptides Into Nonadhesive Hydrogels Useful for Tissue Resurfacing. *Journal of Biomedical Materials Research* 39 (2),266-276.

33. Honda, H. (1971). Description of the Form of Trees by the Parameters of the Tree-like Body: Effects of the Branching Angle and the Branch Length on the Shape of the Tree-like Body. *J. Theor. Biol.*, 31, 331–8.

34. Hutmacher, D. W, Schantz, T., Zein, I., Ng, K. W., Teoh, S. H., Tan, K. C.(2001). Mechanical Properties and Cell Cultural Response of Polycaprolactone Scaffolds Designed and Fabricated via Fused Deposition Modeling. *J. Biomed. Mate.r Res.,*55:203–16.

35. Ishaug-Riley, S. L., Crane, G. M., Gurlek, A., Miller, M. J., Yasko, A. W., Yaszemski, M. J., Mikos, A. G. (1997). Ectopic Bone Formation by Marrow Stromal Osteoblast Transplantation Using Poly(DL-lactic-co-glycolic acid) Foams Implanted Into the Rat Mesentery. *J. Biomed. Mater. Res.,* 36, 1-8.

36. Itoga, K., Kobayashi, J., Yamato, M., Kikuchi, A., & Okano, T. (2006). Maskless Liquid-Crystal-Display Projection Photolithography for Improved Design Flexibility of Cellular Micropatterns. *Biomaterials*, 27, 3005–9.

37. Kaihara, S., Borenstein, J., Koka, R., Lalan, S., Ochoa, E.R., Ravens, M., Pien, H., Cunningham, B., & Vacanti, J. P. (2000). Silicon Micromachining to Tissue

Engineer Branched Vascular Channels for Liver Fabrication. *Tissue Eng.*, 6, 105–117.

38. Karch, R., Neumann, F., Neumann, M., Schreiner, W.(2003). Voronoi Polyhedra Analysis of Optimized Arterial Tree Models. *Annals of Biomedical Engineering,* 31(5), 548-563.

39. Korff, T., & Agustin, H.G.(1998). Integration of Endothelial Cells in Multicellular Spheroids Prevents Apoptosis and Induces Differentiation. *J. Cel.l Bio.,l* 143, 1341.

40. Landers, R., Hu¨bner, U., Schmelzeisen, R., & Mu¨ lhaurpt, R. (2002). Rapid Prototyping of Scaffolds Derived From Thermoreversible Hydrogels and Tailored for Applications in Tissue Engineering. *Biomaterials,* 4437-47.

41. Langer, R. (2000).Tissue engineering. *Molecular Therapy,* Vol. 1 No. 1.

42. Langer, R., Vacanti, J. P., (1993). Tissue Engineering. *Science*,920-926.

43. Lars, M., Yvette, E., Brendan, L., Enrico, C., & Przemyslaw, P. (2005). Quantitative Modeling of Arabidopsis Development. *Plant Physiology*, 139,960-968.

44. Linsen, L., Karis. B. J., McPherson, E. G., & Hamann, B. (2005). Tree Growth Vsualization. *J. WSCG,* 13, 81–8.

45. Lu, Y., Mapili, G., Suhali, G., Chen, S., & Roy, K. (2005). A Digital Micro-mirror Device-based System for the Microfabrication of Complex, Spatially Patterned Tissue Engineering Scaffolds. *J. Biomed. Mater. Res.*, A 77, 396–405

46. Lu, L., & Mikos, A. G. (1996). The Importance of New Processing Techniques in Tissue Engineering. *Mater. Res. Soc. Bull,*. 21(11):28-32.

47. Ma, P. X. (2004). Scaffolds for tissue fabrication. *Mater. Today*, 30-40.

48. Khalil, S., Nam, J., & Sun, W. (2005). Multi-nozzle Deposition for Construction of 3D Biopolymer Tissue Scaffolds. *Rapid Prototyping Journal,* 9–17.

49. Mann, B.K., Gobin, A.S., Tsai, A. T., Schmedlen, R. H., & West, J. L. (2001). Smooth Muscle Cell Growth in Photopolymerized Hydrogels With Cell Adhesive and Proteolytically Degradable Domains: Synthetic ECM Analogs for Tissue Engineering. *Biomaterials*, 22,3045-3051.

50. Mann, B.K., & West. J. L. (2002). Cell Adhesion Peptides Alter Smooth Muscle Cell Adhesion, Proliferation, Migration, and Matrix Protein Synthesis on Modified Surfaces and In Polymer Scaffolds. *J.Biomed. Matter. Res.* 60,86-93.

51. Mann, B.K., Schemedlen, R. H., & West J. L (2001). Tethered-TGF-β Increases Extracellular Matrix Production of Vascular Smooth Muscle Cells in Peptide-modified Scaffolds. *Biomaterials*, 22,439-44.

52. Měch, R., & Prusinkiewicz, P. (1996). Visual models of plants interacting with their environment. *Proceedings of SIGGRAPH New Orleans, LA,* 397-410.

53. Metters, A. T., Anseth, K.S., Bowman, C. N. (1999) Fundamental Studies of biodegradable hydrogels as cartilage replacement materials. *Biomed. Sci. Instrum,*35,33-38.

54. Halstenberg, S., Panitch, A.,Rizzi S., Hall, H., Hubbell, J.A.(2002). Biologically Engineered protein-graft-poly(ethylene glycol)hydrogels: A cell adhesive and plasmin-degradable biosynthetic material for tissue repair. *Biomacromolecules*,3, 710-723.

55. Mikos, A. G., Thorsen, A. J., Czerwonka, L. A., et al. (1994). Preparation and Characterization of Poly(L-lactic acid) Foams. *Polymer* 35:1068-1077.

56. Mooney, D. J., Baldwin, D. F., Suh, N. P., Vacanti, J. P., Langer, R. (1996). Novel Approach to Fabricate Porous Sponges of poly(D,L lactic co-glycolic acid) without the Use of Organic Solvents. *Biomaterials,* 1417-1422.

57. Nelson, C. M., & Tien, J. (2006). Microstructured Extracellular Matrices in Tissue Engineering and Development. *Curr. Opin. Biotechnol.,* 17, 518–523.

58. Napolitano, A. P., Dean, D. M., Man, A J., Youssef. J., Ho, D. N., Rago, A P., Lech, M. P., & Morgan, J.R. (2007). Scaffold–free Three-dimensional Cell Culture Utilizing Micromolding Non-adhesive Hydrogels. *Biotechniques* 43,494-500.

59. Northrop, J. H., and Kunitz, M.(1926). The Swelling Pressure of Gelatin and the Mechanism of Swelling in Water and Neutral Salt Solutions. *J. Gen Physiol.,*10,161-177.

60. Northrop, J. H., Kunitz, M.(1926). The Swelling and Osmotic Pressure of Gelatin in Salt Solutions. *J. Gen Physiol.,*317-337.

61. Ma, P. X. (2004). Scaffolds for Tissue Fabrication. *Materials Today* 30-40.

62. Poncelet, D., Neufeld, R. J., Goosen, M. F. A., Burgarski, B., & Babak, V. (1999). Formation of Microgel Beads by Electric Dispersions. *American Institute of Chemical Engineers,* 2018-23.

63. Prusinkiewicz, P., & Lindenmayer, A. (1990). The Algorithmic Beauty of Plants (Berlin: Springer)

64. Prusinkiewicz, P. (1993). Modeling and Visualization of Biological Structures. *Proc. Graphics Interface*, 128–37.

65. Prusinkiewicz, P., Hammel., M, Hannan, J., & Mech, R. (1996). Visual Models of Plant Development. In: Rozenburg, G., and Salomaa, A. (Eda.): *Handbook of Formal Languages*, Spriner-Verlag, Berlin,535-597.

66. Painter, P. R., Eden, P., Bengtsson, H. (2006). Pulsatile Blood Flow, Shear Force, Energy Dissipation and Murray's Law. *Theoretical Biology and Medical Modelling,* 3-31.

67. Rago, A. P., Chai, P. R., and Morgan, J. R. (2009). Encapsulated Arrays of Self-assembled Microtissues: an alternative to spherical microcapsules.*Tissue Engineering Part A,* 387-95.

68. Rahman, T. M., Selden, C., Khalil, M., Diakanov, I., and Hodgson, H. J. F. (2004). Alginate Encapsulated Human Hepatoblastoma Cells in an Extracorporeal Perfusion System Improve Some Systematic Parameters of Liver Failure in a Xenogenic Model. *Artif. Organs*, 476,482.

69. Ryan, C. M., Carter, E. A., Jenkins, R. L., Sterling, L.M., Yarmush, M. L., Malt, R. A., & Tompkins, R.G. (1993). Isolation and Long-term Culture of Human Hepatocytes. *Surgery*, 48-54.

70. Reuber, M., Yu, L. S., Kolff, W. J., (1987). Effect of Processing Temperature on the Properties of Polyurethone and Comparison of Vacuum Forming and Solution Casting to Make Artificial Hearths. *Artif. Organs*, 323-323.

71. Roy, P., Baskaran, H., Tilles, A. W., Yarmush, M. L., Toner, M. (2001). Analysis of Oxygen Transport to Hepatocytes in a Flat-plate Microchannel Bioreactor.
Ann Biomed Eng.,947-55.

72. Sachlos, E., & Czernuszka, J. T. (2003). Making Tissue Engineering Scaffolds Work. *Europeans cells and materials*, 29-44.

73. Schmitz, J. P., Hollinger, J. O. (1988). A Preliminary Study of the Osteogenic Potential of a Biodegradable Alloplastic-osteoinductive Alloimplant. *Clin Orthop*, 245-255.

74. Starly, B., and Sun, W.(2007). Internal Scaffold Architecture Designs using Lindenmayer Systems, *J. of Computer Aided Design and Applications*,395-403.

75. Starly, B., Lau, W., Bradbury, T., and Sun, W. (2006). Internal Architecture Design Methodology for Tissue Replacement Structures. *Computer Aided Design*, 115-124.

76. Sun, C., Fang, N., Wu, D. M., and Zhang, X. (2005). Projection Micro-stereolithography Using Digital Micro-mirror Dynamic Mask. *Sensors Actuators A*, 113–20.

77. Svendsen, C. N., Ter-Borg, M. G., Armstrong, R. J., Rosser, A. E., Chandran, S., Ostenfeld, T., and Caldwell, M. A. (1998). A New Method for the Rapid and Long Term Growth of Human Neural Precursor Cells. *J. Neurosci Methods,* 141-152.

78. Sumide, T., Nishida, K., Yamato, M., Ide, T., Hayashida, Y., Watanabe, K., Yang, J., Kohno, J., Kikuchi, A., Maeda, N., Watanabe, H., Okano, T., Tano, Y. (2006). Functional Human Corneal Endothelial Cell Sheets Harvested from Temperature-responsive culture Surfaces. *The FASEB Journal,* 392-394.

79. Tilles, A. W., Baskaran, H., Roy, P., Yarmush, M. L., Toner, M. (2001). Effects of Oxygenation and Flow on the Viability and Function of Rat Hepatocytes Cocultured in a Microchannel Flat-plate Bioreactor. *Biotechnol Bioeng.,*379-89.

80. Underhill, G. H., Chen, A. A., Albrecht, D. R., & Bhatia, S. N. (2007). Assessment of Hepatocellular Function Within PEG Hydrogels. *Biomaterials*, 256–70.

81. Vacanti, J. P., & Lange, R. (1999). Tissue Engineering: The Design and Fabrication of Living Replacement Devices for Surgical Reconstruction and Transplantation. *Lancet,* 32-4.

82. Valerie, A., Buijs, J. D., Bajzer, Z., Ritman, E. L., (2006). Branching Morphology of the Rat Hepatic Portal Vein Tree: A Micro-CT Study. *Annals of Biomedical Engineering,* 1420-1428.

83. Valerie, A. L., & Sangeeta, N. B. (2002). Three Dimensional Photopaterning of Hydrogels Containing Living Cells. *Biomedical Microdevices*, 257-266.

84. Vernon, R. B., Gooden, M. D., Lara, S. L., andWight, T. N. (2005). Native Fibrillar Collagen Membranes of Micro-scale and Sub-micron Thickness for Cell Support and Perfussion. *Biomaterials,* 1109–1117.

85. Vozzi, G., Previti, A., de Rossi, D. and Ahluwalia, A. (2002). Microsyringe-based Deposition of Two-dimensional and Three-dimensional Polymers Scaffolds With a Well-defined Geometry for Application to Tissue Engineering. *Tissue Engineering,* 1089-98.

86. Vozzi, G., Previti, A., Ciaravella, G., and Ahluwalia, A. (2004). Microfabricated Fractal Branching Networks. *J. Biomed. Mater. Res. A,* 326–33.

87. Vozzia, G., Flaimb, C., Ahluwaliaa, A., Bhatiab, S. (2003). Fabrication of PLGA Scaffolds Using Soft Lithography and Microsyringe Deposition. *Biomaterials*, 2533–2540.

88. Vozzi, G., Chiono, V., Ciardelli, G., Giusti, P., Previti, A., Cristallini, C., Barbani, N., Tantuss, G., and Ahluwalia, A. (2004). Microfabrication of Biodegradable Polymeric Structures for Guided Tissue Engineering. *Mat. Res. Soc. Symp. Proc*,1-3.

89. Yang, S., Kah, F., and Zhaohui, D. (2001). The Design of Scaffolds for Use in Tissue Engineering . Part I. Traditional Factors. *Tissue Engineering*, 679-689.

90. Yasar, O., Lan, S., and Starly, B. (2009). A Lindenmayer System-based Approach for the Design of Nutrient Delivery Networks in Tissue Constructs. *Biofabrication*, 1-9.

91. Starly, B., Chang, R., and Sun, W (2006). UV-Photolithography Fabrication of Poly-Ethylene Glycol Hydrogels Encapsulated with Hepatocytes. *Proceedings of 17th Solid Freeform Fabrication Symposium*, August 14-16th, 2006, Austin, TX, USA

92. Khalil, M., Panahi, A. S., Tootle, R., Ryder, T., McCloskey, P., Roberts, E., Hodgson, H., Selden, C. (2009). Human Hepatocyte Cell Lines Proliferating as Cohesive Spheroid Colonies in Alginate Markedly Upgregulate Both Synthetic and Detoxificatory Liver Function. *J. Hepotol,*387-95.

93. Kim, B. S., Mooney, D. J. (1998). Development of biocompatible synthetic extracellular matrices for tissue engineering. *Trends Biotechnol.*, 224–230.

94. Geckil, H., Xu, F., Zhang, X., Moon, S., & Demirci, U. (2010). Engineering Hydrogels as Extracellular Matrix Mimics. *Nanomedicine*, 469–484.

95. Wang, F., Shor, L., Darling, A., Khalil, S., Sun, W., Gu̇çeri, S., and Lau, A. (2004). Precision Extruding Deposition and Characterization of Cellualr Poly-1-caprolactone Tissue Scaffolds. *Rapid Prototyping Journal,* 42-9.

96. Williams, C. G., Kim, T. K., Taboas, A., Malik, A., Manson, P., and Elisseef, J. (2003). In Vitro Chondrogenesis of Bone Marrow Derived Mesenchymal Stem Cells in a Photopolymerizing Hydrogel. *Tissue Eng.*, 679-688.

97. Won-Shik, C., Sung-Geun, K., Woo-Kyun, J., Hyung-Jung, K., and Sung-Hoon, Ahn. (2007). Fabrication of Micro Parts Using Nano Composite Deposition System. *Rapid Prototyping Journal*, 276–283.

98. Zamir, M. (2001). Arterial Branching Within the Confines of Fractal L-System Formalism. *J. Gen. Physiol.*, 267–75.

99. Zein, I., Hutmacher, D. W., Tan, K. C., & Teoh, S. H. (2002). Poly(e-caprolactone) Scaffolds Designed and Fabricated by Fused Deposition Modeling. *Biomaterials*,1169-1185.

100. Lam, C. X. F. , Mo, X. M., Teoh, S. H., Hutmacher, W. (2002). Scaffold Development Using 3D printing With a Strach-based Polymer. *Mater. Sci. Eng. C*,49-56.

101. Zeltinger J, Sherwood JK, Graham DA, Mueller R, Griffith LG. Effect of pore size and void fraction on cellular adhesion, proliferation, and matrix deposition. Tissue Eng 2001;7:557–72.